Holocene vegetation and climate dynamics of NE China based on the pollen record from Sihailongwan Maar Lake

Martina Stebich [a, *], Kira Rehfeld [b], Frank Schlütz [a, c], Pavel E. Tarasov [d], Jiaqi Liu [e], Jens Mingram [f]

[a] Senckenberg Research Station of Quaternary Palaeontology Weimar, Am Jakobskirchhof 4, 99423 Weimar, Germany
[b] Alfred Wegener Institute, Helmholtz Centre for Polar and Marine Research, Telegrafenberg A43, 14473 Potsdam, Germany
[c] Lower Saxony Institute for Historical Coastal Research, Viktoriastr. 26/28, 26382 Wilhelmshaven, Germany
[d] Institute of Geological Sciences, Palaeontology Section, Free University Berlin, Malteserstr. 74–100, Haus D, 12249 Berlin, Germany
[e] Institute of Geology and Geophysics Chinese Academy of Sciences, No.19 Beitucheng West Road, Chaoyang District, Beijing, 100029, China
[f] GFZ German Research Centre for Geosciences, Section 5.2 - Climate Dynamics and Landscape Evolution, Telegrafenberg C109, 14473 Potsdam, Germany
* Corresponding author. Tel.: +49 3643 493093332; fax: +49 3643 493093352.
E-mail address: martina.stebich@senckenberg.de (M. Stebich).

Abstract

High-resolution palynological analysis on annually laminated sediments of Sihailongwan Maar Lake (SHL) provides new insights into the Holocene vegetation and climate dynamics of NE China. The robust chronology of the presented record is based on varve counting and AMS radiocarbon dates from terrestrial plant macro-remains. In addition to the qualitative interpretation of the pollen data, we provide quantitative reconstructions of vegetation and climate based on the method of biomization and weighted averaging partial least squares regression (WA-PLS) technique, respectively. Power spectra were computed to investigate the frequency domain distribution of proxy signals and potential natural periodicities. Pollen assemblages, pollen-derived biome scores and climate variables as well as the cyclicity pattern indicate that NE China experienced significant changes in temperature and moisture conditions during the Holocene. Within the earliest phase of the Holocene, a large-scale reorganization of vegetation occurred, reflecting the reconstructed shift towards higher temperatures and precipitation values and the initial Holocene strengthening and northward expansion of the East Asian summer monsoon (EASM). Afterwards, summer temperatures remain at a high level, whereas the reconstructed precipitation shows an increasing trend until approximately 4000 cal. yr BP. Since 3500 cal. yr BP, temperature and precipitation values decline, indicating moderate cooling and weakening of the EASM. A distinct periodicity of 550-600 years and evidence of a Mid-Holocene transition from a temperature-triggered to a predominantly moisture-triggered climate regime are derived from the power spectra analysis. The results obtained from SHL are largely consistent with other palaeoenvironmental records from NE China, substantiating the regional nature of the reconstructed vegetation and climate patterns. However, the reconstructed climate changes contrast with the moisture evolution recorded in S China and the mid-latitude (semi-)arid regions of N China. Whereas a clear insolation-related trend of monsoon intensity over the Holocene is lacking from the SHL record, variations in the coupled atmosphere-Pacific Ocean system can largely explain the reconstructed changes in NE China.

Keywords: Holocene pollen, biomes and climate reconstruction, spectral analysis, East Asian summer monsoon

Highlights:

- Holocene vegetation and climate dynamics in NE China are studied.
- Climate shifts are revealed through palynology and biome/climate reconstructions.
- Asynchronous maximums in the Holocene summer temperature and monsoon precipitation.
- Pacific sea ice extent and sea surface temperatures influence climate in NE China.

1. Introduction

The East Asian summer monsoon (EASM) plays a major role in the global climate system (Wang, 2009). In mid-latitude and southern Asia, ecosystems, rain-fed agriculture and economic prosperity critically depend on the amount and distribution of monsoonal precipitation (Yasuda and Shinde, 2004). Therefore, detailed knowledge of the monsoon system variability is essential for understanding global climate processes and is of societal and economic interest, particularly with regard to existing uncertainties in future rainfall projections (Stocker et al., 2013).

A large number of palaeoenvironmental records have already been generated to better understand the spatio-temporal variability and control mechanisms of the Asian monsoon (e.g. Wang et al., 2010; Cao et al., 2013; Ran and Feng, 2013; An, 2014; Yang et al., 2014). In general, these studies primarily invoke local or regional moisture changes as most indicative of variations in monsoon strength and large-scale circulation patterns. Particularly, oxygen isotope records from speleothems in S/E China have substantially influenced palaeo-monsoon research as they are well dated and widely considered to be high-resolution summer monsoon proxies (e.g., Wang et al., 2005; Liu et al., 2014). The basic idea of orbitally forced insolation change as the main driver of the Asian summer monsoon intensity over the Holocene has been supported by stalagmite oxygen isotopic values roughly tracking the precession cycle (e.g. Wang et al., 2005). Likewise, investigations on vegetation response to climate changes appear to corroborate humid Early to Mid-Holocene and drier conditions during the Late Holocene, suggesting a similar moisture evolution across the monsoon-influenced regions of China (Zhao et al., 2009a; Zhang et al., 2011; Ran and Feng, 2013).

However, other studies point to much more variability of the summer monsoon in space and time. In particular, towards its northern margin, proxy records reveal region-specific palaeoenvironmental changes, suggesting a complex interplay between the Indian summer monsoon (ISM), the EASM and other major climatic factors, including topography and vegetation (Hu et al., 2003; Maher and Hu, 2006; An et al., 2006; Zhao and Yu, 2012; Ran and Feng, 2013).

To reveal coherent spatio-temporal patterns of climate evolution in monsoonal Asia and adjacent regions, available proxy data were used for summarizing compilations, over-regional correlations, for constructing 'monsoon/moisture indices' and data-model comparisons (An, 2000; Ren and Beug, 2002; Morrill et al., 2003; An et al., 2006; Herzschuh, 2006; Chen et al., 2008; Zhao et al., 2009a,b; Cai et al., 2010; Wang et al., 2010; Kleinen et al., 2011; Zhao and Yu, 2012; Cao et al., 2013, Dallmayer et al., 2013; Leipe et al., 2014; Yang et al., 2014). However, the regional behaviour of the summer monsoon and its over-regional linkages is far from being well understood. This is reflected in ongoing debates regarding (i) the regional impact of the major atmospheric circulation systems controlling moisture distribution patterns in China (e.g. Clemens et al., 2010; An et al., 2012; Ran and Feng, 2013), (ii) the phase relationships between these systems (e.g. He et al., 2004; Zhao et al., 2009a; Wang et al., 2010; Cai et al., 2010; Clemens et al., 2010; Zhang et al., 2011; An et al., 2012; Ran and Feng, 2013; Li et al., 2014; Yang et al., 2014), and (iii) the role of other factors, including ocean-atmosphere interactions, solar activity, and high-low-latitude interactions, on the regional climate (e.g. An, 2000; Wang and Qian, 2009; Caley et al., 2014; Jin et al., 2014). With the aim to decipher the continental-scale monsoon dynamics new statistical approaches were developed (e.g. Clemens et al., 2010; Rehfeld et al., 2012; Donges et al., 2015). However, precisely dated high-resolution palaeoenvironmental records are still insufficient (Zhao et al., 2009a,b; Zhang et al., 2011; Donges et al., 2015; Chen et al., 2015). For NE China, which is located in a key geographical position at the northern periphery of the EASM, between the semi-arid regions of northern China and the Pacific Ocean, wealthy evidence of Holocene vegetation and climate changes has become available in recent years (e.g. Hong et al., 2001; Ren, 2007; Jiang et al., 2008; Makohonienko et al., 2008; Chen et al., 2015). Annually laminated sediments recovered from maar lakes of the Longgang Volcanic Field (LVF, Fig. 1C) offer excellent opportunities for detailed palaeoenvironmental reconstructions with a temporal resolution of few years to several decades and an excellent time control far back into the last glacial (Mingram et al., 2004; Schettler et al., 2006; Stebich et al., 2007, 2009; Chu et al., 2011, 2014; You and Liu, 2012; Li et al., 2013; Zhu et al., 2013; Xu et al., 2014). However, interpretation results presented in these publications are not always consistent. Considering multiproxy evidence (pollen and geochemical data), You and Liu (2012) reported an increasing Holocene temperature trend from 11,400 cal. yr BP and "optimum climate condititions" between 4200 and 1670 cal. yr BP, while Chu et al. (2014) identified an increasing lake level from 9000-4000 cal. yr BP and a stably high lake level afterwards. On the other hand, evidence of eight severe drought periods during the past 6000 cal. yr BP were derived from the $\delta^{13}C$ time-series of peat cellulose recovered from the nearby Hani peat (Hong et al., 2001). Multidecadal to multicentennial-scale cold/warm fluctuations were deduced from pollen data for the past 5300 cal. yr BP (Xu et al., 2014), from alkenone based temperature reconstructions for the past 1600 cal. yr BP (Chu et al., 2011), and from multi-proxy analysis for the entire Holocene (You et al., 2012). However, the reconstructed shifts and short-term events appear not always synchronous and yield different cyclicity patterns. The previous findings from NE China imply that during the Holocene both rainfall and temperature play a substantial and most probably changing role in shaping regional climate and vegetation pattern. In addition, different sensitivity of each proxy to the air temperature and precipitation changes possibly affect interpretations and may lead to vague or inconsistent conclusions regarding changes in the monsoon system (Ren and Zhang, 1998; Schettler, 2011; Stebich et al., 2011; Ran and Feng, 2013).

In this paper, we present a new high-resolution palynological record from the Holocene sedimentary section of Sihailongwan Maar Lake (SHL), NE China. A robust reconstruction of vegetation and climate dynamics, at first is based on a detailed palaeoecological discussion of the pollen assemblages. To facilitate a more reliable separation of the recorded temperature and moisture changes, we conducted biome and quantitative climate reconstructions and power spectrum analyses. The biome reconstruction reveals dominant vegetation surrounding the study site through time and provides an excellent opportunity to cross-validate the quantitatively reconstructed climate variables. Finally, we critically discuss the reconstructed temperature and precipitation trends derived from the SHL pollen record in comparison with other palaeoclimate records and possible forcing mechanisms.

2. Regional settings

Lake Sihailongwan (42°17’ N, 126°36’ E) is an extant maar lake within the Longgang Volcanic Field situated in the Changbai Mountains region, Jilin Province, NE China (Fig. 1A). The nearly circular lake is located at 797 m a.s.l., has a maximum water depth of approximately 50 m and a diameter of 720 m. The lake surface area (ca. 0.4 km^2) and its relatively small catchment (ca. 0.7 km^2) are appropriate for recording mainly a regional signal in the pollen record (Prentice, 1985). The crater’s walls rise up to 121 m above the current lake level. The lake is mainly fed by summer rainfall, in conjunction with associated groundwater inflow, and does not have inflowing or outflowing streams (Schettler et al., 2006). The study region is characterized by a sub-humid, temperate climate that is mainly controlled by the EASM (Wang and Lin, 2002). At the closest meteorological station at Jingyu town (ca. 20 km NE of the lake), the mean annual temperature (Tann) averages at 2.5°C, with a mean coldest month (January) temperature (Mtco) of -18.1°C and mean warmest month (July) temperature (Mtwa) of 20.7 °C. The mean annual precipitation (Pann) is 775 mm, with up to 71% of it falling from May to August (Table 1; Schettler et al., 2006;

Chu et al., 2011). The interannual variability of the summer rainfall is relatively large, co-influenced by the mid-latitude and tropical circulation dynamics (Lee et al., 2005; Shen et al., 2011).

The earliest Neolithic archaeological sites recorded in Liaoning and the Liao River regions, NE China, date back to ca. 7500 cal. yr BP (Wagner et al., 2013 and references therein) or even earlier and represent Xinlongwa pottery culture largerly sustained on hunting, fishing and gathering (Liu and Chen, 2012; Wagner and Tarasov, 2014). The gradual transition to farming began in the Changbai region approximately 5000 cal. yr BP, whereas scattered wood-cutting tools were found in this region from 4000 cal. yr BP. At approximately 2000 years ago, crop cultivation is estimated to have reached 50% of the local economy, while a number of wall fortresses were built in this area (Jia, 2005). There is documentary evidence of a territorial expansion of the Tang Dynasty, including farming activities, in the study region approximately 1300 years ago (Jiang et al., 2008 and references within). Nevertheless, the land in the Changbai Mountains region was assumed to be relatively pristine before the Qing Dynasty (1616-1912 AD) because natural vegetation was well preserved by the emperors as traditional Manchurian land and imperial hunting ground in the early Qing Dynasty (Zhang, 2000).

The study area belongs to the modern temperate conifer-hardwood forest zone (Fig. 1B), representing one of the main preserved woodland areas in China today. Major constituents of the species-rich natural forests include *Quercus mongolica*, *Tilia mandshurica*, *T. amurensis*, *Acer mono*, *Fraxinus mandshurica*, *Juglans mandshurica*, *Carpinus cordata*, *Phellodendron amurensis*, *Maackia amurensis*, *Pinus koraiensis*, *P. densiflora*, *Abies nephrolepis*, and *Picea jezoensis* (Qian et al., 2003). The current knowledge of modern forest vegetation in NE China is based on numerous botanical and ecophysiological studies (Qian et al., 2003; Krestov et al., 2006; Wang et al., 2006; Yu et al., 2011, 2013; Zhang et al., 2014). Ecological investigations of recent vegetation distribution and tree species with respect to climate indicate that temperature and precipitation during the growing season and potential evapotranspiration are key factors responsible for the spatial differentiation of modern vegetation in NE China (Jiang et al., 2008; Wang et al., 2009, Zhang et al., 2014, Zheng et al., 2014; Li et al., 2015). Large-scale analysis of the modern pollen distribution and its quantitative relationship with vegetation and climate in China and E Asia demonstrate that hydrological variables are more important than temperature-related variables in determining the pollen assemblage composition in NE China (Li et al., 2015). However, the bioclimatic tolerance of regional forest trees given by Fang et al. (2009) show significant overlap, which requires a critical discussion of palaeoclimatic implications.

Forests, surrounding SHL, were cut down completely during the 1970s. Since then, a largely undisturbed succession has taken place, yielding recent canopy coverage of 80–90%. Pioneer species as *Betula costata*, *B. platyphylla*, *Populus davidiana* and *P. ussuriensis* are dominant. Other temperate trees are still young, mainly occurring in the shrub layer together with typical shrubs, including species of *Euonymus*, *Philadelphus*, *Actinidia*, *Syringa*, *Lespedeza*, *Sorbaria* and *Lindera*. On the upper slopes of the crater, conifers (*Abies nephrolepis*, *Picea jezoensis*, *Pinus koraiensis*, *P. massoniana*) are more abundant.

3. **Material and Methodology**

3.1. *Sediment recovery and dating*

Several sediment cores up to 39 m long were recovered from the SHL at three adjacent drilling sites in 2001 using a high-precision piston coring system (Mingram et al., 2007). Overlapping sediment sequences were used to define a continuous composite profile which is almost completely seasonally laminated (Schettler et al., 2006). The varves are of mixed organogenic/minerogenic composition, with diatom frustules representing the dominant biogenic silica contributor to the sediment (Mingram et al., 2004). Analyses of sediment microfacies and varve counting are based on 10-cm-long, overlapping petrographic thin-sections, which were prepared by applying the freeze-drying method after Merkt (1971). Varve counts uncertainties were addressed by multiplying with a correction factor of 1.0622, which was derived from a linear regression function between the original varve ages and 40 calibrated AMS ^{14}C dates of terrestrial plant remains. Radiocarbon ages within the range of INTCAL09 for the Holocene and the younger part of the Late-glacial are listed in Schettler et al. (2006). Radiocarbon datings of the older part (prior to ca. 15,000 cal. yr BP) and the age-depth model are discussed in full detail in Stebich et al. (2009). All ages are given in calibrated years before present (cal. yr BP).

3.2. *Pollen analysis*

Pollen samples were taken volumetrically from the composite profile at 2-cm intervals, beginning at a composite depth of 18 cm (150 cal. yr BP) down to 4.37 m (12,000 cal. yr BP), thus providing an average temporal resolution of ca. 55 years. *Lycopodium* spores were added to each sample to calculate pollen concentrations. Preparation of pollen samples involved treatment with HCl, KOH, HF and hot acetolysis mixture, following standard methods described by Berglund and Ralska-Rasiewiczowa (1986). Sample residues were stained with safranine and mounted in glycerine. A minimum of 535 pollen grains (620 pollen grains in average) of terrestrial plant taxa were counted for each sample. Pollen grains of wetland and water plants as well as any type of non-pollen palynomorphs (NPP: spores, algae, zoological remains) are excluded from the pollen sum. Palynomorph identification was carried out with the aid of palynological reference collections of the Senckenberg Research station for Quaternary Palaeontology and of Frank Schlütz, supported by pollen atlases (Beug, 2004; Li, 2011; Wang et al., 1995). The work of van Geel and Aptroot (2006) provided detailed information for identification of fungi spores.

3.3. Biome reconstruction

The commonly accepted biome reconstruction technique (Prentice et al., 1996) was used to identify major vegetation units based on the assignment of pollen taxa to plant functional types (PFTs) and to biomes, taking into account the modern ecology, bioclimatic tolerances and geographical distribution of the pollen-producing plants. Concept and the procedure of the biomization technique are described in Prentice et al. (1996) and Prentice and Webb (1998). The method has been successfully tested with surface pollen data from eastern Eurasia (Yu et al., 2000; Mokhova et al., 2009; Chen et al., 2010; Tarasov et al., 2013; Ni et al., 2014). Assignment of the identified pollen taxa in the SHL record to one or more PFTs follows the regional biomization schemes given by Yu et al. (2000) and Chen et al. (2010) for China and Mokhova et al. (2009) for the Russian Far East. As suggested by Prentice et al. (1996), a universal threshold of 0.5% was applied to all terrestrial pollen taxa of the SHL record to minimize possible noise due to long-distance transport, redeposition of exotic pollen grains or misidentification of rare pollen taxa. Affinity scores of each potential biome were then calculated for each fossil pollen spectrum and biome with the highest score was assigned to the respective spectrum (see Prentice et al., 1996 for detail explanation of the method). All calculations were performed using the PPPBase software developed by Guiot and Goeury (1996). Bioclimatic limits of PFTs and related biomes are used to interpret the results of pollen-based biome reconstruction in terms of past climate features (Prentice et al., 1992; Harrison et al., 2010). Basically, this method allows identifying only the biome that has the highest affinity with the studied pollen assemblage at a certain time, but not the reconstruction of transitional vegetation types. Nevertheless, we also include subordinate biome scores in the interpretation to recover this information to some extent and to support palaeoclimatic interpretations (Tarasov et al., 2013).Additional information concerning the vegetation cover (i.e. landscape openness) was obtained by calculating the difference between the maximum forest biome score and the maximum open biome score for the analysed pollen assemblages (Tarasov et al., 2013).

3.4. *Climate reconstruction*

Quantitative climate reconstructions were performed using weighted-averaging partial least squares (WA-PLS) regression (ter Braak and Juggins, 1993) with two components. WA-PLS has been shown to be a robust method for obtaining transfer functions that copes well with noisy datasets with autocorrelation and large environmental gradients (ter Braak and Juggins, 1993; Birks, 1998; Telford and Birks, 2009). The calibration model was established by Cao et al. (2014) using modern pollen samples from 2559 sites in Mongolia and China, and monthly climate data (i.e. Tann, Mtco, Mtwa and Pann) was derived from meteorological observations. The calibration data set covers a large precipitation and temperature range, and encloses modern values at the SHL site in its midst (Table 1). Additionally, we have checked that the closest modern analogues of the fossil data are all within the modern calibration set. The WA-PLS2 model showed robustness against spatial autocorrelation, tested by deleting modern pollen samples at random and close to the cross-validation site (Cao et al., 2014).

Reconstructions for the SHL fossil pollen record were performed using the open-source software R (*rioja* package; Juggins, 2012). Model performance was evaluated using the package *palaeoSig* (Telford, 2012). The function randomTF in the software package paleoSig performs a constrained ordination on the fossil data using reconstructed climate variables. This yields the proportion of explained variance of the individual reconstructions. In our case, these are 40 and 35 % for Mtwa and Pann, respectively. In a second step, transfer functions are developed based on random data, in order to evaluate how much variance is explained by such transfer functions. This yields a null distribution of explained variances, and based on this null distribution, critical values can be defined, and p-values computed. The computed p-values are 0.02 for Mtwa (i.e. the reconstruction of Mtwa explains more variance than 98% of the random transfer functions) and 0.12 for Pann (i.e. it is better than 88% of random transfer functions), whereas the Mtco and Tann p-values explain less variance than that of the Mtwa and are strongly collinear with it. Because the precipitation reconstruction explains less variance than the reconstructed temperatures, it should be treated with more caution.

3.5. *Spectral analysis*

Power spectra for the reconstructed climatic variables (Pann, Mtwa) and for the most indicative tree pollen taxa (*Pinus*, *Betula*, *Juglans* and *Quercus*) were computed to investigate the frequency domain distribution of the signal and potential periodicities. All time series were square-root-transformed and then detrended using a 2000-year timescale Gaussian kernel highpass filter prior to the analysis. The data series were interpolated to the tenfold sampling rate and then lowpass-filtered to the original sampling timescale. They were then interpolated to a regular mean spacing of 60.5 years to prevent aliasing of high-frequency variability in the spectrum. We then computed the power spectra using the well-known multitaper method (Thomson, 1990) with three windows. Because the skewness of the sampling rate distribution is close to zero, the effect of time series irregularity on the spectrum is low (Rehfeld et al., 2011; Rehfeld and Kurths, 2014). Continuous locally white noise background spectra were obtained by robustly smoothing the multitaper spectrum with a 21-point running median, tapering down to 11 points at the edges. Local confidence levels were estimated from this background using the 90% critical values of a Chi-Squared distribution with six degrees of freedom (Mann and Lees, 1996).

4. **Results and discussion**

4.1. *Pollen pattern and regional vegetation development*

In total, 120 pollen and spore taxa and 31 non-pollen palynomorph (NPP) types were distinguished in the Holocene SHL section. Most arboreal pollen taxa (AP) occur with values of at least 0.5% and are present throughout the whole sequence. Except for *Artemisia* and Chenopodiaceae, non-arboreal pollen (NAP) taxa occur scattered or in small quantities, ranging between 0 and 0.5%. Excluding *Botryococcus* algae, NPP are detected in trace amounts. Total pollen concentration is extremely high, ranging from ca. 60,000 to 2.9 million grains per cm^3 sediment, with a mean of approximately 500,000 grains per cm^3.

Beginning with the late Younger Dryas (YD) period, the pollen diagram covers the period between 12,000–150 cal. yr BP (Fig. 2). The diagram has been simplified to include only most conclusive taxa, and it overlaps with sections presented in Mingram et al. (2004) and Stebich et al. (2009). The Holocene sequence was visually divided into four pollen assemblage zones (SHL-H1 to SHL-H4) based on major changes in pollen assemblage composition and ecological and climatic characteristics of the dominant taxa. Similar to today's regional forest vegetation, the percentage values of main tree pollen taxa in the SHL core sediment — *Pinus haploxylon*-type (*Pinus koraiensis*), *Picea*+*Abies*+*Larix*, *Betula*, *Ulmus*, *Fraxinus*, *Quercus*, *Juglans*, *Carpinus*, and *Tilia* — indicate polydominant forest vegetation in the study area of NE China during almost the entire Holocene. Changes in pollen percentages reflect a development from open Late-glacial woodland to mesophytic deciduous forest and, finally, to the present mixed conifer and broadleaf deciduous forest vegetation.

4.1.1. Establishment of broadleaved deciduous forests (SHL-H 1: 11,650 – 10,700 cal. yr BP)

During the final stage of the Younger Dryas, the region near SHL was occupied by boreal woodland with occasional elements of (cool-)temperate forest (Stebich et al., 2009).

During the first millennium of the Holocene (11,650-10,700 cal. yr BP), the boreal vegetation was successively replaced by species-rich broadleaf deciduous forests, representing a transitional stage. The interglacial vegetation succession begins with an increase in *Betula* and a stepwise reduction in cold-tolerant conifers (*Picea+Abies+Larix*), followed by a progressive increase in *Ulmus* and *Fraxinus* and a substantial decline of *Betula* at approximately 11,250 cal. yr BP. The latter change marks the final transformation of the Late-glacial open vegetation into the Holocene interglacial forest-dominated landscape. Contemporaneously, other deciduous taxa become successively more common or reach their empirical limit (i.e. *Quercus*, *Juglans*, *Tilia*, *Vitis*, and *Viburnum*). The frequencies of most herbaceous taxa (i.e. *Artemisia*, Poaceae, Cyperaceae, *Thalictrum,* and *Sanguisorba officinalis*) gradually decline, indicating a progressive increase in forest cover density and a reduction in open habitats/forest gaps as a result of shading by spreading trees. It is likely that the initial Holocene vegetation development was somewhat protracted by interspecific competition with established conifers and *Betula* trees and the delayed immigration of some warm-loving tree species. Nevertheless, the vegetation development implies that growing conditions had already become favourable for establishing temperate trees at 11,650 cal. yr BP (Stebich et al., 2009), clearly reflecting a trend towards relatively warm and moist climate conditions during the first millennium of the Holocene.

4.1.2. Establishment and dynamics of oak- and walnut-rich forests (SHL-H2: 10,700–7800 cal. yr BP)

At approximately 10,700 cal. yr BP, the dynamic spread of thermophilous *Juglans* and a more gradual increase of *Quercus* at the expense of *Ulmus* and *Fraxinus* mark a shift in the vegetation composition to oak- and walnut-rich temperate broadleaf deciduous forests. Other temperate broadleaf deciduous trees and shrubs, such as *Tilia*, *Carpinus* and *Corylus*, become slightly more abundant. Boreal conifers virtually disappear from the study region as indicated by only scattered occurrences of conifer pollen (i.e. *Haploxylon*-type, *Picea*, *Abies*, *Larix*) and the absence of their stomata from the sediment. At approximately 9750 cal. yr BP, the increase of *Quercus* combined with the decline of *Betula* possibly indicates a vegetation succession from birch-rich pioneer woods to oak forests. Later on, step-wise increase in the *Quercus* pollen percentages indicates further spread of oaks in the study area at approximately 9100 and 8100 cal. yr BP, each time following a short-term *Juglans* maximum. The Early Holocene series of rapid fluctuations in tree pollen abundances ends with a marked decline in *Juglans* pollen percentages shortly after 8200 cal. yr BP. This decline is followed by a sharp increase in *Quercus* and, afterwards, in *Ulmus* and *Fraxinus* percentages.

The modern temperate broadleaf deciduous forests in NE China mainly comprise various species, including *Quercus*, *Juglans*, *Ulmus*, *Tilia*, *Carpinus*, *Acer*, *Corylus*, *Populus*, *Betula* and some *Pinus*. These species grow south of the mixed conifer-hardwood forests under a (warm-) temperate climate (Ren and Beug, 2002). Conifers are restricted in NE China to colder conditions of higher elevations and/or higher latitudes (Liu, 1997; Qian et al., 2003). Thus, their virtual absence in the Early Holocene pollen assemblages points to climatic conditions warmer than today. The spread of dense forests in the study region since the Early Holocene is supported by low pollen contribution of steppe and meadow elements (e.g. *Artemisia*, Chenopodiaceae, *Thalictrum*, Poaceae, and Cyperaceae). Accordingly, an annual precipitation exceeding 500 mm can be supposed for the SHL region. At present, the two most common oak species in the region, *Quercus mongolica* and *Q. dentata*, are forming mixed mesophytic forests (Cui et al., 2002; Qian et al., 2003). In fact, both oak species can tolerate a wide range of habitat conditions and are able to adapt to cold and drought climates (Cui et al., 2002; Qian et al., 2003; Fang et al., 2009; Šrůtek et al., 2003). The recently widespread *Quercus mongolica* is a canopy species extensively growing on shady slopes (Cui et al., 2002). *Juglans mandshurica* occurs in NE China at lower elevations, in valleys, along rivers, and on gentle slopes with deep, well-drained soils (Qian et al., 2003). The fast-growing walnut tree is less drought tolerant than the above mentioned oak species (Cui et al., 2002; Fang et al., 2009). We therefore hypothesise that the increasing *Quercus*/stagnating *Juglans* proportions indicate drought stress on the forest vegetation during the Early Holocene. The contemporaneous decreasing trend in *Artemisia* may reflect a progressive spreading of forest vegetation into the west-adjacent steppe region, where patches of mixed pine and broadleaved forests became established during a mild, but relative dry climate between 10,250 and 7900 cal. yr BP (Xu et al., 2010). In addition, short excursions in the *Juglans* and *Quercus* pollen point to recurrent spells of diminished monsoon intensity.

4.1.3. Spreading of *Pinus koraiensis* (SHL-H3: 7800–5200 cal. yr BP)

The beginning of the Middle Holocene interval is marked by a rapid increase of *Juglans* with maximum pollen percentage values at 7800 cal. yr BP. Because *Juglans* tends to be underrepresented in the pollen assemblages from lake sediments, values of 15-25% indicate a temporary dominance of walnut in the regional forests (Beer et al., 2007). In addition, *Carpinus* trees become slightly more common, possibly filling forest gaps and shading out the lianas of wild wine species (*Vitis* type pollen) but remaining a subordinate forest element until recent times. According to Wang et al. (2006), the distribution of *Carpinus cordata* is less climatically controlled, while competition seems to be a more important ecological factor for this species. The overall frequencies of herb pollen reach their lowest Holocene values, indicating maximum forest coverage and increasing wetness.

From about 6600 cal. yr BP, the steady increase of the *Pinus haploxylon*-type implies the immigration of *Pinus koraiensis*, a recently widespread tree in the study region at elevations between 740-1450 m a.s.l. This species occurs in late stages of forest succession (Qian et al., 2003; Yu et al., 2011) and represents a characteristic species of the modern broadleaf and needle-leaf mixed forests of NE China. Attributing the high values of the *Haploxylon*-type pollen to *Pinus pumila*, the only other pine of that pollen type in NE China, seems unlikely. *Pinus pumila* in this part of Asia represent a subalpine shrub growing above 1700 m a.s.l., together with grasses and herbs (Zhu et al., 2003). Thus, the remaining low NAP percentages and high values of mesophytic trees argue against the establishment of such an open vegetation type near the study site. Several studies are characterizing *Pinus koraiensis* as a species with a relatively narrow ecological capacity for moisture adaptation (Wei et al., 1995; Chen and Li, 2005; Yu et al., 2013). It grows on well-drained soils, but low precipitation has been identified as an important limiting factor, especially at its southern geographic and lower altitudinal limits (Wang et al., 2004; Yu et al., 2013 for discussion and references). Considering the elevation of SHL and its location near the southern limit of the Korean pine distribution area, the immigration of *Pinus koraiensis* implies that sufficiently humid conditions persisted during the Mid-Holocene.

4.1.4. Establishment and dynamics of the recent mixed coniferous hardwood forests (SHL – H4: 5200–150 cal. yr BP)

An increase in *Pinus haploxylon*-type pollen to more than 25% documents a substantial spread of *Pinus koraiensis* at approximately 5200 cal. yr BP. Since then, the mesophytic broadleaf deciduous forests with *Juglans* and *Quercus* never again dominated in the regional vegetation cover, while *Pinus koraiensis* likely became one of the most common tree species in the SHL region. Later, the spreading of birch forests and *Artemisia* steppes most likely implies a shift to drier conditions. Beginning at 3500 cal. yr BP, *Artemisia* percentages fluctuate between 10% and 20%. Such values likely yield a remote signal of *Artemisia* steppes (Beer et al., 2007) and may reveal a substitution of forests by *Artemisia* steppes in dry habitats, particularly in the forest-steppe ecotone west of the SHL region under increasingly dry climate conditions. The rapid increase in birch pollen percentages points to decreasing forest density and/or drier conditions in the study region. The currently common *Betula platyphylla* and *B. dahurica* are drought tolerant and shade intolerant tree species, which are mainly found as pioneer trees on sunny slopes (Chen and Li, 2005). The other common birch species, *Betula costata,* has moderate drought and shade tolerance. The spreading of birch at the expense of pine may thus reflect drier conditions and/or substantial ecosystem disturbances. From 2900 cal. yr BP, cold tolerant conifer taxa started to become more frequent forest elements, indicating climate cooling. Concomitantly, role of broadleaf trees such as *Ulmus*, *Fraxinus*, and *Juglans* further decrease, while birches as well as steppe elements such as *Artemisia*, *Thalictrum,* and Chenopodiaceae show increase. Palynological evidences of local water and wetland vegetation (e.g. *Alisma*, *Equisetum*, *Hippuris*, *Myriophyllum*, *Sphagnum*, *Batrachium*, *Lysimachia*, *Parnassia*, *Persicaria maculosa,* and *Potamogeton* types) are very sparse or missing. Approximately 950 years ago, *Fraxinus* retreated again, while cold-tolerant conifers further expanded in the SHL region, pointing to a continued cooling trend with possibly shorter growing period. Forests were, if at all, only slightly replaced by herbaceous vegetation types and human-induced changes cannot be traced. However, sporadically occurring pollen grains of *Xanthium strumarium* type may indicate an anthropogenic introduction of this annual weedy species at 2100 cal. yr BP (Chen and Hind, 2011). First occurrence of *Xantium strumarium* pollen coincides with archaeological evidence of intensified farming activities between 2000 and 1800 cal. yr BP (Jia, 2005). This may have taken place in conjunction with fires and modest grazing, as evidenced by more frequent occurrence of burnt Poaceae phytoliths (not shown), *Pteridium* spores and coprophilous fungi (*Sporormiell*a, *Cercophora*, and *Sordaria* types). Slightly higher Chenopodiaceae percentage values might also be related to minor human disturbances.

4.2 Biomes, landscape openness and reconstructed climate variables

During the past 12,000 years, either the cool mixed forest biome (COMX) or temperate deciduous forest biome (TEDE) attain highest affinity scores based on the pollen assemblages, while taiga (TAIG), cool coniferous forests (COCO) and steppe (STEP) gain only subordinate biome scores (Fig. 3). A summary of dominant plant types and climatic requirements of the calculated SHL biome scores is presented in Table 2. Biomization results show that at the end of the Younger Dryas, COMX was the dominant vegetation type in the SHL region. COMX consists of boreal and temperate conifers mixed with temperate broadleaf trees and shrubs. It occurs in climates with moderately cold winters (-2 to -15°C), including sufficient heat accumulation during the growing season for broadleaf deciduous trees and sufficient precipitation amounts for boreal conifers (Prentice et al., 1992). Nevertheless, (cool-)temperate trees may also grow under lower winter temperatures (up to -26 °C; Mokhova et al., 2009) if sufficient snow cover is protecting them. The affinity scores of cool coniferous forests (COCO) are slightly lower during the last phase of the Younger Dryas at SHL, corroborating a substantial presence of boreal trees in the vegetation. In addition, the calculated scores of TAIG and STEP and the maximal landscape openness imply mixed regional vegetation cover with drought- and cold-tolerant trees and herbaceous communities playing a considerable role. Correspondingly, Mtwa with ca. 15-16°C and Pann with ca. 300-400 mm were reconstructed, indicating rather weak EASM (Fig. 3).

During the subsequent interval (11,650 to 10,700 cal. yr BP), COMX remained the dominant biome. However, substantial changes in the biome scores are found, i.e. the decrease in STEP, followed by a sudden decrease in TAIG and increase in TEDE. Contemporaneously, denser forest coverage progressively develops. This major vegetation change is clearly reflected in the reconstructed climate variables, indicating a warmer than today Mtwa, whereas precipitation only moderately increases during this time.

Between 10,700 and 5200 cal. yr BP, the TEDE biome is reconstructed as dominant vegetation type. The dominant TEDE constituents are temperate summergreen, cool-temperate conifer and boreal summergreen trees. This biome typically indicates mean winter temperatures higher than -2°C and fairly high summer temperatures, but it can also occur in areas with colder winters (down to -15°C, as in contemporary NE China), where conditions are too dry for boreal evergreen conifers (Prentice et al., 1992). Considering the modern Mtco of -18°C in the study region and the low Early Holocene winter insolation, insufficient moisture availability for boreal evergreen conifers appears to be the main cause of the TEDE biome dominance. Affinity scores of the cold and drought tolerant TAIG and STEP biomes progressively decrease to minimum values, whereas forest coverage reaches its highest density during the Middle Holocene (8000–3500 cal. yr BP). Between 6000 and 5000 cal. yr BP, the COMX biome successively replace the TEDE biome, marking a long-term transition to modern vegetation and climate conditions. Because COMX contains temperate broadleaf trees and shrubs mixed with boreal and temperate conifers, the reconstructed regional vegetation trend suggests successively increasing effective moisture during the Early and Middle Holocene. After 3500 cal. yr BP, the reconstructed biomes and landscape openness indicate a pronounced environmental shift. At that time, increasing affinity scores of cold and drought-tolerant biomes (TAIG, STEP) and declining TEDE scores imply a significant summer monsoon weakening and probably lower winter temperatures.

In line with the calculated biome affinity scores, the reconstructed climate variables show a constantly high Mtwa (about 5°C higher than today) between 11,250 and 3500 cal. yr BP and increasing Pann values until the Middle Holocene. Starting at 3500 cal. yr BP, reconstructed Mtwa and Pann values decrease to recent levels. Although COMX remains the dominant vegetation type during the Late Holocene, short-term fluctuations in biome scores and reconstructed climate variables corroborate increased climate variability. The reconstructed climate changes also led to a substantial decrease in regional forest coverage, as suggested by the biome-derived estimation of landscape openness and higher frequencies of *Pteridium aquilinum* spores. While reconstructed Late Holocene precipitation values fluctuate around modern mean Pann value, reconstructed Mtwa ranges slightly above the modern mean value. Tao et al. (2010) simulated increased Mid-Holocene summer temperatures 2-3°C higher than the pre-industrial value for N and NE China. For the Mid-Holocene thermal optimum, existing proxy-based temperature reconstructions from China reveal 1-4°C (regionally even >4°C) higher annual/seasonal surface air temperatures than during the pre-industrial period (Shi et al., 1993; Tang et al., 2000; He et al., 2004; Ljungqvist, 2011), thus supporting our reconstruction derived from the SHL record.

4.3. Periodic multi-centennial oscillation pattern of pollen and climate variables

The SHL pollen assemblages exhibit fluctuations implying centennial-scale climate variations superimposed on the gradual Holocene vegetation and climate trends discussed above. During the Early Holocene, short-term *Juglans* maxima appear, whereas substantial decreases in *Pinus haploxylon* pollen perecntages, coupled with percentage maximums of drought-tolerant *Quercus*, *Betula* and *Artemisia*, indicate noticeable changes in composition and structure of *Pinus koraiensis* mixed forests during the Late Holocene. Because substantial human impact seems rather unlikely in the region before 1300 cal. yr BP, the vegetation changes are most likely related to natural environmental changes. Several studies demonstrate that insufficient rainfall and soil water stress can be considered as key limiting factors for *Juglans mandshurica* and *Pinus koraiensis* growth (Zhao et al., 1991; Wang et al., 2004; Fang et al., 2009; Yu et al., 2011, 2013) in the study region, despite the relatively humid character of the modern climate. Minimum temperatures in winter could likewise be responsible for decreasing *Juglans* values during the Early Holocene (Zhao et al., 1991).

Spectral analyses performed on reconstructed Pann and Mtwa and on most indicative tree pollen taxa percentages reveal a distinct and significant periodicity of 550-600 years for temperature, precipitation (Fig. 4A), and for *Pinus* and *Betula* time series during the past 10,000 years. When slightly shifted towards longer periods, the peak is also consistently detected for variations in *Quercus* and *Juglans*. Although, several spectral peaks resemble those of known solar cycles, they do not necessarily imply a mechanistic link between vegetation dynamics and solar activity. Rather, non-linear signal transfer seems to be the main reason for individual cyclic changes in the percentage value of each pollen taxon. Beyond climate forcing, other mechanisms, such as fire, competition and natural forest regeneration cycles may generate different quasi-periodic forest composition changes at decadal to millennial time scales (Green et al., 1981). Only the shared periodicity of 550-600 years, which is apparent in most of the pollen taxa curves and in reconstructed climate variables, suggests an underlying climate forcing.

A 550-600-year cycle has been noted previously from other Holocene palaeoclimate records of the Asian monsoon region, e.g. the Heshang HS4 and Dongge DA stalagmites (Cosford et al., 2008; Liu et al., 2012) and plant cellulose from peat deposits in NE China (Hong et al., 2001), whereas Xu et al. (2014) reported a 500-year periodicity for the pollen record from Xiaolongwan. In addition, cycles of 400-600 years have been observed in the NW Pacific, while the N Atlantic record of sediment colour and slope sediments of the Great Bahama Bank also yield periodicities centred at 550 years and 500-600 years, respectively (Chapman and Shackleton, 2000; Roth and Reijmer, 2005; Gorbarenko et al., 2014). This 500-600-year oscillation is argued to reflect the dynamics of atmospheric and oceanic processes, which might be amplified by solar output (Neff et al., 2001; Roth and Reijmer, 2005; Liu et al., 2008; Gorbarenko et al., 2014).

Motivated by the fact that different pollen taxa exhibiting high-frequency shifts in their relative values during the Early and Late Holocene, we split the time series at 5000 cal. yr BP for subsequent analyses of 0-5000 cal. yr BP and 5-10,000 cal. yr BP periods (Figs. 4B, C). As a result, an approximately 500-year periodicity appears for the reconstructed Early Holocene temperature, while a corresponding frequency is missing in the precipitation reconstruction. Conversely, precipitation reveals a significant 500-550-years periodicity during the Late Holocene, whereas a corresponding feature is lacking for the temperature reconstruction. It therefore appears that the NE China region may have gradually shifted from a primarily temperature-controlled vegetation development during the warm Early Holocene to a predominantly monsoonal-rainfall-controlled vegetation change during the humid Late Holocene.

4.4. Sihailongwan climate changes in the context of East Asian terrestrial palaeomonsoon records

Comparison of reconstructed climate variables from SHL with stalagmite records from S and E China shows a close match between the Mtwa long-term trend in NE China and the precession-driven changes in the cave oxygen isotopes, while the precipitation curve from NE China displays a different pattern (Figs. 5). At the beginning of the Holocene, stalagmite oxygen isotopes and the SHL Mtwa reveal a marked shift, indicating a contemporaneous transition from a glacial to interglacial climate in both regions. However, our pollen-based Pann reconstruction exhibits a less-pronounced increase at approximately 11,250 cal. yr BP, suggesting a modest shift towards increased summer monsoon-associated rainfall at SHL. Likewise, the subsequent precipitation trend at SHL does not follow the classical concept of an early to Mid-Holocene precipitation maximum in the realm of the EASM but reveals long-term increasing rainfall up to a maximum value centred at 4000 cal. yr BP. Thereafter, temperature and precipitation reconstructions imply a gradual weakening of the EASM activity in NE China, while the effective moisture remains at a relatively high level probably due to decreasing Late Holocene temperatures. These results largely correspond to the steady increase of effective rainfall in NE China during the past 9000 years derived from lipid biomarkers of neighbouring Xiaolongwan Maar Lake (Chu et al., 2014), substantiating the regional nature of this palaeoclimate pattern. Furthermore, low frequency of peatland initiation during the Early Holocene and highest swamp formation rates between 4200 and 800 yr BP (Xing et al., 2015) are consistent with our reconstructed Holocene moisture evolution in NE China. Similar to SHL vegetation and climate development patterns are also recorded in other nearby palaeoecological archives for the second half of the Holocene (e.g., Jinchuan Peat:

Makohonienko et al., 2008; Jingpo Lake: Chen et al., 2015). In particular, the close similarity between the pollen records from SHL and Xiaolongwan (Xu et al., 2014) confirms the regional-scale nature of multi-centennial changes during the past 5000 years, depite some inconsistencies in the timing of centennial events recorded in both archives. A long-term increasing Holocene precipitation trend is also evident in several pollen-based rainfall reconstructions from the eastern Tibetan Plateau (Wang et al., 2014). Although an Early Holocene moisture shift at approximately 11,250 cal. yr BP is missing from most proxy records from N China (e.g., Hulun Lake: Wen et al., 2010; Daihai Lake: Xu et al., 2010; Luanhaizi Lake: Wang et al., 2014; Gonghai Lake: Chen et al. 2015), there are basic similarities between the reconstructed precipitation and moisture evolution at SHL and that from (semi-)arid regions of northern/central China and interior Asia, i.e. Mid-Holocene humidity maximum and drier conditions afterwards (Fig. 5).

The validity of speleothem oxygen isotope records as proxy for summer monsoon intensity is still a matter of debate (Caley et al., 2014). Whereas Liu et al. (2014) claim that $\delta^{18}O$ records represent the intensity of the EASM system, a study of Yang et al. (2014) reveals that rainfall variability in the ISM region primarily controls the isotopic composition of Chinese cave stalagmites. A pollen based reconstruction of ISM precipitation from NW China (Xingyun Lake: Chen et al. 2014) widely parallels the stalagmite $\delta^{18}O$ trend and supports the hypothesis published by Yang et al. (2014). In this respect, the different trends observed in the rainfall records from NE China and in the oxygen isotopic composition derived from the Dongge stalagmites argue for an asynchrony in the ISM and the extratropical EASM evolution. Nevertheless, Caley et al. (2014) doubt the validity of Asian speleothem oxygen isotopes to represent summer monsoon strength due to the complex influences modulating the monsoonal precipitation pattern and the $\delta^{18}O$ composition in cave stalagmites.

Using additional $\delta^{18}O$-independent proxy data (including pollen), Ran and Feng (2013) provide regionally-averaged moisture indices, which reveal a bell-shaped Holocene humidity maximum in northern China (including NE China) between 9500 and 5000 cal. yr BP and a plateau-shaped moisture optimum in S China between 11,000 and 4000 cal. yr BP. Based on the different curve patterns they infer that the EASM strength had gradually transgressed northward during the Early Holocene and gradually regressed southward during the Late Holocene. However, the Holocene moisture trend reported by the recent studies in NE China (Chu et al., 2014; Xing et al., 2015; Chen et al., 2015; this study) does not support the reconstruction by Ran and Feng (2013). Moreover, our pollen-based vegetation and climate reconstructions and the spectral analysis results, strongly suggest that monsoonal precipitation and insolation-driven temperature changes co-determine the environmental dynamics in NE China. This may explain present inconsistencies among available data sets in NE China and beyond and call for critical (re)-assessment of proxies used to infer changes in monsoon strength and in large scale circulation processes. Given the rather dry climate in arid Central Asia, N and NE China during the Early Holocene, some authors (An et al., 2012; Zhao and Yu, 2012) hypothesized that the climate near the modern monsoon margin was co-controlled by strong and/or dry westerlies, restricting the northward movement of the subtropical monsoon rainfall belt during this time. Zhao and Yu (2012) explained such strong westerly influence by the extant ice sheets in N America and N Eurasia and low sea-surface temperatures (SSTs) in the N Atlantic Ocean responsible for low evaporation and reduced water transport to the Eurasian continent. However, SSTs registered in various North Atlantic records show an Early Holocene maximum, challenging this hypothesis. Instead, Chen et al. (2008) suppose that the mid-latitude westerlies could have been enhanced through a large meridional temperature gradient during the Early Holocene. In contrast, Jin et al. (2012) attribute Early Holocene aridity in Central Asia to a reduction of moisture advection brought by weak westerly winds and decreased upstream evaporation, which are primarily related to winter conditions. Independent evidence of enhanced influence from the Asian interior, at least during the winter/spring seasons, is derived from maximum remote dust accumulation rates recorded in the SHL sediments between 11,000 and 8200 cal. yr BP (Zhu et al., 2013). Following Zhu et al. (2013), the increased Early Holocene dust transport into the SHL region could result from increased insolation-driven seasonality with lower winter and higher summer temperatures in arid and semi-arid mid-latitude regions of China and Mongolia as well as from increased meridional temperature gradients. As a result, a high frequency of cold air surges and enhanced cyclone activity occur in these regions promoting springtime dust storms in NE China.

The absence of dust layers in the SHL sediment after 8000 kyr BP may reflect a basic change in the atmospheric circulation and/or increasing vegetation coverage in the dust source region at that time. The moist Middle Holocene at SHL coincides with the humidity maximum along the northern margin of the EASM and in arid Central Asia (Chen et al., 2008; Wen et al., 2010; Xu et al., 2010; Zhao and You, 2012), indicating the northernmost Holocene impact of the EASM in the Asian mid-latitudes at that time. The climate optimum was followed by moderate cooling starting in NE China at approximately 3500 cal. yr BP, when similar to modern vegetation and climate conditions became established (Fig. 5). The cooling and drying trends are reconstructed in the entire EASM domain, thus, different precipitation trends reported for N/NE and S China are no longer obvious. We interpret this change as regime shift associated with a significant monsoon weakening, during which the northern limit of the summer monsoon moved to the south and the effective rainfall substantially decreased.

4.5. Sihailongwan climate changes in the light of Pacific Ocean influences

In addition to the insolation-driven thermal land-sea contrast and the position and strength of Northern Hemisphere westerlies, changes in the coupled atmosphere-Pacific Ocean system are considered key factors influencing the seasonal migration of the subtropical monsoonal precipitation front as well as the regional rainfall distribution within China (Ding and Chan, 2005). In particular, prevalent blocking highs over Eurasia, spring arctic sea ice and shifts in the W Pacific subtropical high (WPSH; Fig. 1) are known to favour abundant rainfall in NE China (Gao et al., 2014; Guo et al., 2014). Chu et al. (2014) discussed a correlation between rainfall in NE China and the strength of the blocking Okhotsk High, comparing their $\delta^{13}C_{27\text{-}31}$ N-alkane pattern with an alkenone-based SST reconstruction from the mixed water region off Sanriku, in the NW Pacific (Minoshima et al., 2007). Although such a teleconnection is known from recent climate observations (Shen et al. 2011), we cannot find explicit evidence of changes in the Okhotsk High and related monsoon changes in NE China during the Holocene in the SHL records.

Nevertheless, several similarities between reconstructed SHL rainfall trends and proxy records from the Pacific Ocean realm corroborate a major role of the Pacific Ocean in regulating EASM rainfall (Fig. 6). Similar to reconstructed precipitation patterns in NE China, the relative abundance of sea-ice-related diatoms from the W Okhotsk Sea show long-term Early to Middle Holocene increase yielding in a maximum at approximately 4000 cal. yr BP, and decreasing values afterwards (Fig. 6). According to Guo et al. (2014), today's lower-than average spring sea ice in the Arctic is associated with higher precipitation amounts in southern EASM region and less rainfall in the northern EASM region, and vice versa. Thus, observed Holocene precipitation trends in S China *versus* NE China and the presumed sea ice extent in the Okhotsk Sea (Harada et al., 2014) provide support for such driving mechanism throughout the Holocene. However, given the complex spatio-temporal variability pattern of proxy records from marine environments, particularly within the Pacific Arctic, shortcomings still exist in dating uncertainties and data interpretation (Max et al., 2012; Juggins, 2013; Harada et al., 2014). Uncovering this high-low-latitude climate linkage remains a significant challenge and should be additionally tested by palaeoclimate simulations.

In addition to sea ice extent, SSTs reconstructed from Mg/Ca ratios from the northern East China Sea also exhibit obvious parallels with reconstructed Holocene precipitation amounts at SHL (Fig. 6; Kubota et al., 2010, 2015). Even taking into account the chronological limitations of the marine record, both data sets show a quasi-simultaneous shift towards a stronger EASM at the beginning of the Holocene and a similar trend afterwards. However, the reconstructed high SHL Mtwa and high SSTs compared with moderately increasing Early Holocene rainfall suggest that the SHL region may be co-influenced by insolation increase during summer, or even by dry westerlies, while the monsoonal precipitation increase is not able to compensate the enhanced evaporation. Considering the recent linkages between SSTs in the subtropical W Pacific, the WPSH and the moisture transport from oceans to inland regions, it is likely that the shift of SSTs in the NW Pacific at the beginning of the Holocene induced a north-/westward displacement of the WPSH. Consequently, the monsoon precipitation extended to NE China and caused the initial Holocene rainfall increase (Liu et al., 2008; Shen et al., 2011; Deng et al., 2014; Yang et al., 2014). Analogously, the subsequent millennial-scale rainfall trend in NE China follows variations in the subtropical W Pacific.

4.6. Conclusions

In this paper we present a new detailed palynological data set covering the Holocene part of the annually laminated sediments from Sihailongwan Maar Lake, NE China. Conventional interpretation of the SHL pollen assemblages is complemented by the results of quantitative biome and climate reconstructions and power spectrum analysis. The reconstructed climate variables are then validated statistically and by comparison with the regional and extra-regional records.

The pollen-based biome reconstruction indicates that the study region was covered by COMX and TEDE forests during the past 12,000 cal. yr BP. According to bioclimatic limits of reconstructed biomes, significant shifts in affinity scores represent changes in regional thermal and hydrological conditions, in agreement with reconstructed climate variables. Prior to the Holocene onset, the Mtwa and Pann values were ca. 6-7°C and 300-400 mm lower than today, suggesting rather weak EASM activity. A constantly high summer temperature is reconstructed between 10,700 and 3500 cal. yr BP, while precipitation slowly increases during the Early and Mid-Holocene towards its maximum at approximately 4000 cal. yr BP. Since 3500 cal. yr BP, Mtwa and Pann decrease to recent levels, while effective humidity remains high, and unstable environmental conditions are reconstructed. A distinct and statstically significant periodicity of 550-600 years has been identified for reconstructed climate variables during the last 10,000 years. From different power spectra patterns of reconstructed Mtwa and Pann during the first and second half of the Holocene, we infer a shift in main driving factors influencing vegetation and/or climate evolution and a partial decoupling of temperature and rainfall in NE China. These results are largely consistent with other data from NE China.

Comparisons with other proxy records from the EASM monsoon domain reveal that the reconstructed SHL climate development differs from the Holocene moisture evolution recorded in δ18O records from E and S China stalagmites and in mid-latitude arid regions of northern China. The reconstructed SHL precipitation points towards a continuous northward advance of the EASM during the Early and Middle Holocene, whereas a clear insolation-related trend of monsoon intensity during the Holocene is missing for NE China. In the Early Holocene, prevailing dry westerlies may have co-influenced the climate in NE China. On the other hand, we have found strong similarities between the Holocene moisture development in NE China and palaeoclimate proxies from the NW Pacific Ocean, which reflect close coupling of the atmosphere-Pacific Ocean system. In future data syntheses and modelling studies, NE China should therefore be regarded as separate climate region. Moreover, asynchronous temperatures and precipitation trends in NE China demonstrate that proxy data at least from extratropical monsoon regions could be affected by both variables and may, if considered separately, not necessarily reflect summer monsoon intensity. Our new comprehensive data set from SHL is relevant for data-model comparisons, which in turn may help decipher spatio-temporal patterns and driving forces of climate evolution in monsoonal Asia and adjacent regions.

Acknowledgements

This study contributes to the joint research program CAME (Central Asia and Tibet: Monsoon Dynamics and Geo-Ecosystems) and has been funded by the German Federal Ministry of Education and Research (BMBF) through grant 03G0813C. K. Rehfeld was financially supported by the Initiative and Networking Fund of the Helmholtz Association grant no VG-900NH". Research of P. Tarasov has been supported via the DFG Heisenberg Program (grant TA 540/5). We are grateful to R. Telford (University of Bergen), P. Rioual (CAS, Beijing), T. Utescher (Steinmann Institute, Bonn) as well as U. Herzschuh and X. Cao (both AWI Potsdam) and Y. Hu (GFZ Potsdam) for constructive discussions and suggestions. We thank two anonymous reviewers for their helpful comments.

References

An, C., Feng, Z., Barton, L., 2006. Dry or humid? Mid-Holocene humidity changes in arid and semi-arid China. Quat. Sci. Rev. 25, 351-361.

An, Z., 2000. The history and variability of the East Asian paleomonsoon climate. Quat. Sci. Rev. 19, 171-187.

An, Z. (Ed.), 2014. Late Cenozoic Climate Change in Asia: Loess, Monsoon and Monsoon-arid Environment Evolution. Springer, Dordrecht.

An, Z., Colman, S.M., Zhou, W.,Li, X., Brown, E. T., Jull, A.J.T., Cai, Y., Huang, Y., Lu, X., Chang, H., Song, Sun, Y., Xu, H., Liu, W., Jin, Z., Liu, X., Cheng, P., Liu, Y., Ai, L., Li, X., Liu, X., Yan, L., Shi, Z., Wang, X., Wu, F., Qiang, X., Dong, J., Lu, F., Xu, X.,

2012. Interplay between the Westerlies and Asian monsoon recorded in Lake Qinghai sediments since 32 ka. Sci. Rep. 2, doi: 10.1038/srep00619.

Beer, R., Tinner, W., Carraro, G., Grisa, E., 2007. Pollen representation in surface samples of the Juniperus, Picea and Juglans forest belts of Kyrgyzstan, central Asia. Holocene 17, 599-611.

Berglund, B.E., Ralska-Jasiewiczowa, M., 1986. Pollen analysis and pollen diagrams, in: Berglund, B.E. (Ed.), Handbook of Holocene Palaeoecology and Palaeohydrology. Chichester, Wiley, pp. 455-484.

Beug, H.-J., 2004. Leitfaden der Pollenbestimmung für Mitteleuropa und angrenzender Gebiete. Pfeil, München.

Birks, H.J.B., 1998. Numerical tools in palaeolimnology – progress, potentialities, and problems. J. Paleolimnol. 20, 307-332.

Cai, Y., Tan, L., Cheng, H., An, Z., Edwards, R.L., Kelly, M.J., Kong, X., and Wang, X., 2010. The variation of summer monsoon precipitation in central China since the last deglaciation. Earth Planet Sci. Lett. 291, 21-31.

Caley, T., Roche, D.M., Renssen, H., 2014. Orbital Asian summer monsoon dynamics revealed using an isotope-enabled global climate model. Nat. Commun. 5, doi: 10.1038/ncomms6371.

Cao, X.-Y., Ni, J., Herzschuh, U., Wang, Y.-B., Zhao, Y., 2013. A late Quaternary pollen dataset from eastern continental Asia for vegetation and climate reconstructions: Set up and evaluation. Rev. Palaeobot. Palynol. 194, 21-37.

Cao, X.-Y., Herzschuh, U., Telford, R.J., Ni, J., 2014. A modern pollen–climate dataset fromChina and Mongolia: Assessing its potential for climate reconstruction. Rev. Palaeobot. Palynol. 211, 87-96.

Chapman, M.R., Shackleton, N.J., 2000. Evidence of 550-year and 1000-year cyclicities in North Atlantic circulation patterns during the Holocene. Holocene 10, 287-291.

Chen, F., Chen, J., Holmes, J., Boomer, I., Austin, P., Gates, J.B., Wang, N., Brooks, S.J., Zhang, J., 2010. Moisture changes over the last millennium in arid central Asia: a review, synthesis and comparison with monsoon region. Quat. Sci. Rev. 19, 1055-1068.

Chen, F., Chen, X., Chen, J., Zhou, A., Wu, D., Tang, L., Zhang, X., Huang, X., Yu, J., 2014. Holocene vegetation history, precipitation changes and Indian Summer Monsoon evolution documented from sediments of Xingyun Lake, south-west China. J. Quat. Sci. 29, 661-674.

Chen, F., Yu, Z., Yang, M., Ito, E., Wang, S., Madsen, D., Huang, X., Zhao, Y., Sato, T., Birks, H.J.B., Boomer, I., Chen, J., An, C., Wünnemann, B., 2008. Holocene moisture evolution in arid central Asia and its out-of-phase relationship with Asian monsoon history. Quat. Sci. Rev. 27, 351-364.

Chen, F., Xu, Q., Chen, J., Birks, J.H.B., Liu, J., Zhang, S., Jin, L., An, C., Telford, R.J., Cao, X., Wang, Z., Zhang, X., Selvaraj, K., Lu, H., Li, Y., Zheng, Z., Wang, H., Zhou, A., Dong, G., Zhang, J., Huang, X., Bloemendal, J., Rao, Z., 2015. East Asian summer monsoon precipitation variability since the last deglaciation. Sci. Rep. 4, doi: 10.1038/srep11186.

Chen, R., Shen, J., Li, C., Zhang, E., Sun, W., Ji, M., 2015. Mid- to late-Holocene East Asian summer monsoon variability recorded in lacustrine sediments from Jingpo Lake, Northeastern China. Holocene 25, 454-468.

Chen, X., Li, B., 2005. Spatial variability of plant functional types of trees along Northeast China transect. Appl. Ecol. Environ. Res. 3, 39-49.

Chen, Y., Ni, J., Herzschuh, U., 2010. Quantifying modern biomes based on surface pollen data in China. Glob. Planet. Change 74, 114-131.

Chen, Y., Hind, D.J.N., 2011. Heliantheae, in: Wu, Z.Y., Raven, P.H., Hong, D.Y. (Eds.), Flora of China Volume 20–21 (Asteraceae). Science Press, Beijing & Missouri Botanical Garden Press, St. Louis, pp. 852-878.

Chu, G., Sun, Q., Wang, X., Liu, M., Lin, Y., Xie, M., Shang, W., Liu, J., 2011. Seasonal temperature variability during the past 1600 years recorded in historical documents and varved lake sediment profiles from northeastern China. Holocene 22, 785-792.

Chu, G., Sun, Q., Xie, M., Lin, Y., Shang, W., Zhu, Q., Shan, Y., Xu, D., Rioual, P., Wang, L., Liu, J., 2014. Holocene cyclic climatic variations and the role of the Pacific Ocean as recorded in varved sediments from northeastern China. Quat. Sci. Rev. 15, 85-95.

Clemens, S.C., W.L. Prell, Sun, Y., 2010. Orbital ‐ scale timing and mechanisms driving Late Pleistocene Indo ‐ Asian summer monsoons: Reinterpreting cave speleothem d18O. Paleoceanography 25, PA4207, doi: 10.1029/2010PA001926.

Cosford, J., Qing, H., Eglington, B., Mattey, D., Yuan, D., Zhang, M., Cheng, H., 2008. East Asian monsoon variability since the Mid-Holocene recorded in a high-resolution, absolute-dated aragonite speleothem from eastern China. Earth Planet. Sci. Lett. 275, 296-307.

Cui, H.T., Li, Y.Y., Hu, J.M., Yao, X.S., Li, Y., 2002. Vegetation reconstruction of Bronze Age by using microscopic structure of charcoals. Chin. Sci. Bull. 47, 2014-2017.

Dallmeyer, A., Claussen, M., Wang, Y., Herzschuh, U., 2013. Spatial variability of Holocene changes in the annual precipitation pattern: a model-data synthesis for the Asian monsoon region. Clim. Dyn. 40, 2919-2936.

Deng, Y., Gao, T., Gao, H., Yao, X., Xie, L., 2014. Regional precipitation variability in East Asia related to climate and environmental factors during 1979-2012. Sci. Rep. 4, doi: 10.1038/srep05693.

Ding, Y., Chan, J.C.L., 2005. The East Asian summer monsoon: an overview. Meteorol. Atmos. Phys. 89, 117-142.

Donges, J.F., Donner, R.V., Marwan, N., Breitenbach, S.F.M. , Rehfeld, K., Kurths, J., 2015. Non-linear regime shifts in Holocene Asian monsoon variability: potential impacts on cultural change and migratory patterns. Clim. Past 11, 709-741.

Dykoski, C.A., Edwards, R.L., Cheng, H., Yuan, D., Cai, Y., Zhang, M., Lin, Y., Qing, J., An, Z., Revenaugh, J., 2005. A high-resolution, absolute-dated Holocene and deglacial Asian monsoon record from Dongge Cave, China. Earth Planet. Sci. Lett. 233, 71-86.

Fang, J., Wang, Z., Tang, Z. (Eds.), 2009. Atlas of Woody Plants in China. Vol. 1-3 and index. Higher Education Press, Beijing.

Gao, Y., 1962. On some problems of Asian monsoon, in: Gao, Y. (Ed.), Some Questions about the East Asian Monsoon. Chinese Science Press, Beijing, pp. 1-49 (in Chinese).

Gao, H., Jiang, W., Li, W., 2014. Changed relationships between the East Asian summer monsoon circulations and the summer rainfall in eastern China. J. Meteorol. Res. 28, 1075-1083.

Gorbarenko, S.A., Artemova, A.V., Goldberg, E.L., Vasilenko, Y.P., 2014. The response of the Okhotsk Sea environment to the orbital-millennium global climate changes during the Last Glacial Maximum, deglaciation and Holocene. Glob. Planet. Change 116, 76-90.

Green, D.G., 1981. Time series and postglacial forest ecology. Quat. Res. 15, 265-277.

Guiot, J., Goeury, C., 1996. PPPBASE, a software for statistical analysis of paleoecological and paleoclimatological data. Dendrochronologia 14, 295-230.

Guo, D., Gao, Y., Bethke, I., Gong, D., Johannessen, O.M., Wang, H., 2014. Mechanism on how the spring Arctic sea ice impacts the East Asian summer monsoon. Theor. Appl. Climatol. 115, 107-119.

Harada, N., Katsuki, K., Nakagawa, M., Matsumoto, A., Seki, O., Addison, J. A., Finney, B.P., Sato, M., 2014. Holocene sea surface temperature and sea ice extent in the Okhotsk and Bering Seas. Prog. Oceanogr. 126, 242-253.

Harrison, S.P., Prentice, I.C., Barboni, D., Kohfeld, K., Ni, J., Sutra, J.-P., 2010. Ecophysiological and bioclimatic foundations for a global plant functional classification. J. Veg. Sci. 21, 300-317.

He, Y., Theakstone, W.H., Zhang, Z., Zang, D., Yao, T., Chen, T., Shen, Z., Pang, H., 2004. Asynchronous Holocene climatic change across China. Quat. Res. 61, 52-63.

Herzschuh, U., 2006. Palaeo-moisture evolution at the margins of the Asian monsoon during the last 50 ka. Quat. Sci. Rev. 25, 163-178.

Hong, Y., Jiang, H., Liu, T., Zhou, L., Beer, J., Li, H., Leng, X., Hong, B., Qin, X., 2001. Response of climate to solar forcing recorded in a 6000-yearδ18O time-series of Chinese peat cellulose. Holocene 10, 1-7.

Hu, Z., Yang, S., Wu, R., 2003. Long-term climate variations in China and global warming signals. J. Geophys. Res. 108, doi: 10.1029/2003JD003651.

Jia, W., 2005. Transition from foraging to farming in Northeast China. PhD Thesis, University of Sydney.

Jiang, W., Leroy, S.A.G., Ogle, N., Chu, G., Wang, L., Liu, J., 2008. Natural and anthropogenic forest fires recorded in the Holocene pollen record from a Jinchuan peat bog, northeastern China. Palaeogeogr. Palaeoclimatol. Palaeoecol. 261, 47-57.

Jin, L., Chen, F., Morrill, C., Otto-Bliesner, B.L., Rosenbloom, N., 2012. Causes of early Holocene desertification in arid central Asia. Clim. Dyn. 38, 1577-1591.

Jin, L., Schneider, B., Park, W., Latif, M., Khon, V., Zhang, X., 2014. The spatial-temporal patterns of Asian summer monsoon precipitation in response to Holocene insolation change: a model-data synthesis. Quat. Sci. Rev. 85, 47-62.

Juggins, S., 2012. rioja: Analysis of Quaternary Science Data. version 0.7-3. http://cran.r-project.org/web/packages/rioja/index.html.

Juggins, S., 2013. Quantitative reconstruction in palaeolimnology: new paradigm or sick science. Quat. Sci. Rev. 64, 20-32.

Kleinen, T., Tarasov, P., Brovkin, V., Andreev, A., Stebich, M., 2011. Comparison of modeled and reconstructed changes in forest cover through the past 8000 years: Eurasian perspective. Holocene 21, 723-734.

Krestov, P.V., Song, J., Nakamura, Y., Verkholat, V.P., 2006. A Phytosociological Survey of the Deciduous Temperate Forests of Mainland Northeast Asia. Phytocoenologia 36, 77-150.

Kubota, Y., Kimoto, K., Tada, R., Oda, H., Yokoyama, Y., Matsuzaki, H., 2010. Variations of East Asian summer monsoon since the last deglaciation based on Mg /Ca and oxygen isotope of planktic foraminifera in the northern East China Sea. Paleoceanography 25, PA4205, doi: 10.1029/2009PA001891.

Kubota, Y., Tada, R., Kimoto, K., 2015. Changes in East Asian summer monsoon precipitation during the Holocene deduced from a freshwater flux reconstruction of the Changjiang (Yangtze River) based on the oxygen isotope mass balance in the northern East China Sea. Clim. Past 11, 265-281.

Lee, E.-J., Jhun, J.-G., Park, C.-K., 2005. Remote Connection of the Northeast Asian Summer Rainfall Variation Revealed by a Newly Defined Monsoon Index. J. Clim. 18, 4381-4393.

Leipe, C., Demske, D., Tarasov, P.E., HIMPAC Project Members, 2014. A Holocene pollen record from the northwestern Himalayan lake Tso Moriri: Implications for palaeoclimatic and archaeological research. Quat. Int. 348, 93-112.

Li, J., Xu, Q., Zheng, Z., Lu. H., Luo, Y., Li, X, Li, C., Seppä, H., 2015. Assessing the importance of climate variables for the spatial distribution of modern pollen data in China. Quat. Res. 82, 287-297.

Li, J., Mackay, A.W., Zhang, Y., Li, J., 2013. A 1000-year record of vegetation change and wild fire from maar lake Erlongwan in northeast China. Quat. Int. 290-291, 313-321.

Li, T., 2011. Pollen Flora of China Woody Plants by SEM. Ke xue chu ban she, Beijing (in Chinese).

Li, Y., Wang, N., Zhou, X., Zhang, C., Wang, Y., 2014. Synchronous or asynchronous Holocene Indian and East Asian summer monsoon evolution: A synthesis on Holocene Asian summer monsoon simulations, records and modern monsoon indices. Glob. Planet. Change 116, 30-40.

Liu, H., Lin, Z., Qi, X., Li, Y., Yu, M., Yang, H., Shen, J., 2012. Possible link between Holocene East Asian monsoon and solar activity obtained from the EMD method. Nonlinear Process. Geophys. 19, 421-430.

Liu, J., Wang, B., Yang, J., 2008. Forced and internal modes of variability of the East Asian summer monsoon. Clim. Past 4, 225-233.

Liu, L., Chen, X., 2012. The Archaeology of China. From the Late Paleolithic to the Early Bronze Age. Cambridge World Archaeology. Cambridge University Press, Cambridge.

Liu, Q., 1997. Structure and dynamics of the subalpine coniferous forest on Changbai mountain, China. Plant Ecol. 132, 97-105.

Liu, Z., Wen, X., Brady, E.C., Otto-Bliesner, B., Yu, G., Lu, H., Cheng, H., Wang, Y., Zheng, W., Ding, Y., Edwards, R.L., Cheng, J., Liu, W., Yang, H., 2014. Chinese cave records and the East Asia Summer Monsoon. Quat. Sci. Rev. 83, 115-128.

Ljungqvist, F.C., 2011. The Spatio-Temporal Pattern of the Mid-Holocene Thermal Maximum. Geografie 116, 91-110.

Maher, B.A ., Hu, M., 2006. A high-resolution record of Holocene rainfall variations from the western Chinese Loess Plateau: Antiphase behaviour of the African/Indian and East Asian summer monsoons. Holocene 16, 309-319.

Makohonienko, M., Kitagawa, H., Fujiki, T., Liu, X., Yasuda, Y., Yin, H., 2008. Late Holocene vegetation changes and human impact in the Changbai Mountains area, Northeast China. Quat. Int. 184, 94-108.

Mann, M., Lees, J., 1996. Robust estimation of background noise and signal detection in climatic time series. Clim. Change 33, 409-445.

Max, L., Riethdorf, J. R., Tiedemann, R., Smirnova, M., Lembke-Jene, L., Fahl, K., Nürnberg, D., Matul, A., Mollenhauer, G., 2012. Sea surface temperature variability and sea-ice extent in the subarctic northwest Pacific during the past 15,000 years. Paleoceanography 27, doi: 10.1029/2012PA002292.

Merkt, J., 1971. Zuverlässige Auszählungen von Jahresschichten in Seesedimenten mit Hilfe von Großdünnschliffen. Arch. Hydrobiol 69, 145-154.

Mingram, J., Allen, J.R.M., Brüchmann, C., Liu, J., Luo, X., Negendank, J.F.W., Nowaczyk, N., Schettler, G., 2004. Maar- and crater lakes of the Long Gang Volcanic Field (N.E. China) overview, laminated sediments and vegetation history of the last 900 years. Quat. Int. 123-125, 135-147.

Mingram, J., Negendank, J.F.W., Brauer, A., Berger, D., Hendrich, A., Köhler, M., Usinger, H., 2007. Long cores from small lakes-recovering up to 100 m long lake sediment sequences with a high-precision rodoperated piston corer (Usinger-corer). J. Paleolimnol. 37, 517-528.

Minoshima, K., Kawahata, H., Ikehara, K., 2007. Changes in biological production in the mixed water region (MWR) of the northwestern North Pacific during the last 27 kyr. Palaeogeogr. Palaeoclimatol. Palaeoecol. 254, 430-447.

Mokhova, L., Tarasov, P., Bazarova, V., Klimin, M., 2009. Quantitative biome reconstruction using modern and late Quaternary pollen data from the southern part of the Russian Far East. Quat. Sci. Rev. 28, 2913-2926.

Morrill, C., Overpeck, J.T., Cole, J.E., 2003. A synthesis of abrupt changes in the Asian summer monsoon since the last deglaciation. Holocene 13, 465-476.

Neff, U., Burns, S.J., Mangini, A., Muddelsee, M., Fleitmann, D., Matter, A., 2001. Strong coherence between solar variability and the monsoon in Oman between 9 and 6 kyr ago. Nature 411, 290-293.

Ni, J., Cao, X., Jeltsch, F., Herzschuh, U., 2014. Biome distribution over the last 22,000 yr in China. Palaeogeogr. Palaeoclimatol. Palaeoecol. 409, 33-47.

Prentice, I.C., 1985. Pollen representation, source area, and basin size: Toward a unified theory of pollen analysis. Quat. Res. 23, 76-86.

Prentice, I.C., Guiot, J., Huntley, B., Jolly, D., and Cheddadi, R., 1996. Reconstructing biomes from palaeoecological data: a general method and its application to European pollen data at 0 and 6 ka. Clim. Dyn. 12, 185-194.

Prentice, I.C., Webb, T.III, 1998. BIOME 6000: reconstructing global mid Holocene vegetation patterns from palaeoecological records. J. Biogeogr. 25, 997-1005.

Prentice, I.C., Cramer, W., Harrison, S.P. ,Leemans, R., Monserud, R.A., Solomon, A., 1992. A global biome model based on plant physiology and dominance, soil properties and climate. J. Biogeogr. 19, 117-134

Qian, H., Yuan, X., Chou, Y., 2003. Forest Vegetation of Northeast China, in: Kolbek, J., Šrůtek, M., Box, Elgene E.O. (Eds.), Forest Vegetation of Northeast Asia. Kluwer, Dordrecht, pp. 181-230.

Ran, M., Feng, Z., 2013. Holocene moisture variations across China and driving mechanisms: A synthesis of climate records. Quat. Int. 313-314, 179-193.

Rehfeld, K., Kurths, J., 2014. Similarity estimators for irregular and age-uncertain time series. Clim. Past 10, 107-122.

Rehfeld, K., Marwan, N., Breitenbach, S. F. M., Kurths, J., 2012. Late Holocene Asian summer monsoon dynamics from small but complex networks of paleoclimate data. Clim. Dyn. 41, 3-19.

Rehfeld, K., Marwan, N., Heitzig, J., Kurths, J., 2011. Comparison of correlation analysis techniques for irregularly sampled time series. Nonlinear Process. Geophys. 18, 389-404.

Ren, G., 2007. Changes in forest cover in China during the Holocene. Veg. Hist. Archaeobot. 16, 119-126.

Ren, G., Beug, H.-J., 2002. Mapping Holocene pollen data and vegetation of China. Quat. Sci. Rev. 21, 1395-1422.

Ren, G., Zhang, L., 1998. A preliminary mapped summary of Holocene pollen data for Northeast China. Quat. Sci. Rev. 17, 669-688.

Roth, S., Reijmer, J.J.G., 2005. Holocene millennial to centennial carbonate cyclicity recorded in slope sediments of the Great Bahama Bank and its climatic implications. Sedimentology 52, 161-181.

Schettler, G., 2011. Comment on “Anti-phase oscillation of Asian monsoons during the Younger Dryas period: Evidence from peat cellulose δ13C of Hani, Northeast China” by B. Hong et al. [Palaeogeography, Palaeoclimatology, Palaeoecology 297 (2010) 214-222]. Palaeogeogr. Palaeoclimatol. Palaeoecol. 306, 95-97.

Schettler, G., Liu, Q., Mingram, J., Stebich M., Dulski, P., 2006. East-Asian monsoon variability between 15 000 and 2 000 cal. yr BP recorded in varved sediments of Lake Sihailongwan (northeastern China, Long Gang volcanic field). Holocene 16, 143-157.

Shen, B., Lin, Z., Lu, R., Yi, L., 2011. Circulation anomalies associated with interannual variation of early- and late-summer precipitation in Northeast China. Sci. Chin. Earth Sci. 54, 1095-1104.

Shi, Y., Kong, Z., Wang, S., Tang, L., Wang, F., Yao, T., Zhao, X., Zhang, P., Shi, S., 1993. Mid-Holocene climates and environments in China. Glob. Planet. Change 7, 2019-233.

Šrůtek, M., Kolbek, J., Jarolímek, I., Valachovič, M., 2003. Vegetation-environment Relationships within and among Selected Natural Forests in North Korea, in: Kolbek, J., Šrůtek, M., Box, E.O. (Eds.), Forest Vegetation of Northeast Asia. Kluwer, Dordrecht, pp. 363-382.

Stebich, M., Arlt, J., Liu, J., Mingram, J., 2007. Late Quaternary vegetation history of Northeast China – Recent progress in the palynological investigations of Sihailongwan maar lake. Cour. Forschungsinst. Senckenberg 259, 181-190.

Stebich, M., Mingram, J., Han, J., Liu, J., 2009. Late Pleistocene spread of (cool-) temperate forests in Northeast China and climate changes synchronous with the North Atlantic region. Glob. Planet. Change 65, 56-70.

Stebich, M., Mingram, J., Moschen, R., Thiele, A., Schröder, C., 2011. Comments on “Anti-phase oscillation of Asian monsoons during the Younger Dryas period: Evidence from peat cellulose δ13C of Hani, Northeast China” by B. Hong et al. [Palaeogeography, Palaeoclimatology, Palaeoecology 297 (2010) 214-222]. Palaeogeogr. Palaeoclimatol. Palaeoecol. 310, 464-470.

Stocker, T.F., Qin, D., Plattner, G.-K., Tignor, M., Allen, S.K., Boschung, J., Nauels, A., Xia, Y., Bex, V., Midgley, P.M. (Eds.), 2013. Climate Change 2013: The Physical Science Basis. Contribution of Working Group I to the Fifth Assessment Report of the Intergovernmental Panel on Climate Change. Cambridge University Press, New York.

Tang. L., Shen, C., Liu, K., Overpeck, J.T., 2000. Changes in South Asian monsoon: New high-resolution palaeoclimatic records from Tibet, China. Chin. Sci. Bull. 45, 87-91.

Tao, W., Wang, H., Jiang, D., 2010. Mid-Holocene East Asian summer climate as simulated by the PMIP2 models. Palaeogeogr. Palaeoclimatol. Palaeoecol. 288, 93-102.

Tarasov P.E., Andreev, A.A., Anderson, P.M., Lozhkin, A.V., Leipe, C., Haltia, E., Nowaczyk, N.R., Wennrich, V., Brigham-Grette, J., Melles, M., 2013. A pollen-based biome reconstruction over the last 3.562 million years in the Far East Russian Arctic – new insights into climate-vegetation relationships at the regional scale. Clim. Past 9, 2759-2775.

Telford, R.J., 2012. palaeoSig: Significance tests for palaeoenvironmental reconstructions, version 1.1-1. http://cran.r-project.org/web/packages/palaeoSig/index.html.

Telford, R.J., Birks, H.J.B., 2009. Evaluation of transfer functions in spatially structured environments. Quat. Sci. Rev. 28, 1309-1316.

Thomson, D., 1990. Time series analysis of Holocene climate data. Philos. Trans. R. Soc. A 330, 601-616.

ter Braak, C.J., Juggins, S., 1993. Weighted averaging partial least squares regression (WA-PLS): an improved method for reconstructing environmental variables from species assemblages. Hydrobiologia 269, 485-502.

Van Geel, B., Aptroot, A., 2006. Fossil ascomycetes in Quaternary deposits. Nova Hedwigia 82, 313-329.

Wagner, M., Tarasov, P.E., 2014. The Neolithic of Northern and Central China. In: Renfrew, C., Bahn, P. (Eds.), The Cambridge World Prehistory. Vol. 2. East Asia and the Americas. Part V: 5. Cambridge University Press, pp. 742-764.

Wagner, M., Tarasov, P., Hosner, D., Fleck, A., Ehrich, R., Chen, X., Leipe, C., 2013. Mapping of the spatial and temporal distribution of archaeological sites of northern China during the Neolithic and Bronze Age. Quat. Int. 290–291, 344-357.

Wang, B., Lin, H., 2002. Rainy season of the Asian-Pacific Summer Monsoon. J. Clim. 15, 386-398.

Wang, F., Chien, N., Zhang, Y., Yang, H., 1995. Pollen flora of China. Science Press, Beijing (in Chinese).

Wang, P., 2009. Global monsoon in a geological perspective. Chin. Sci. Bull. 54, 1113-1136.

Wang, X., Fang, J., Sanders, N. J., White, P.S., Tang, Z., 2009. Relative importance of climate vs local factors in shaping the regional patterns of forest plant richness across northeast China. Ecography 32, 133-142.

Wang, X., Tang, Z., Fang, J., 2006. Climatic control on Forests and Tree Species Distribution in the Forest Region of Northeast China. J. Integr. Plant Biol. 48, 778-789.

Wang, Y., Cheng, H., Edwards, R.L., He, Y., Kong, X., An, Z., Wu, J., Kelly, M.J., Dykoski, C.A., Li, X., 2005. The Holocene Asian Monsoon: Links to Solar Changes and North Atlantic Climate. Science 308, 854-856.

Wang, Y., Herzschuh, U., Shumilovskikh, L.S., Mischke, S., Birks, H.J.B., Wischnewski, J., Böhner, J., Schlütz, F., Lehmkuhl, F., Diekmann, B., Wünnemann, B., Zhang, C., 2014. Quantitative reconstruction of precipitation changes on the NE Tibetan Plateau since the Last Glacial Maximum – extending the concept of pollen source area to pollen-based climate reconstructions from large lakes. Clim. Past 10, 21-39.

Wang, Y., Liu, X., Herzschuh, U., 2010. Asynchronous evolution of the Indian and East Asian Summer Monsoon indicated by Holocene moisture patterns in monsoonal central Asia. Earth-Sci. Rev. 103, 135-153.

Wang, Y., Wang, Q., Dai, L., Wang, M., Zhou, L., Dai, B., 2004. Effect of soil moisture gradient on structure of broad-leaved/Korean pine forest in Changbai Mountain. J. For. Res. 15, 119-123.

Wang Z., Qian Y., 2009. The relationship of land-ocean thermal anomaly difference with Mei-yu and South China Sea Summer Monsoon. Adv. Atmos. Sci. 26, 169-179.

Wei, L., Wang, H., Wang, Q., Liu, Y., He, Q., Yuan, J., Shao, H., Song, C., 1995. The influence of climate changes on Korean pine forest in China. Geogr. Res. 14, 17-26 (in Chinese with English abstract).

Wen, R., Xiao, J., Chang, Z., Zhai, D., Xu, Q., Li, Y. C., Itoh, S., 2010. Holocene precipitation and temperature variations in the East Asian monsoonal margin from pollen data from Hulun Lake in northeastern Inner Mongolia, China. Boreas 39, 262-272.

Xing, W., Bao, K., Guo, W., Lu, X., Wang, G., 2015. Peatland initiation and carbon dynamics in northeast China: links to Holocene climate variability. Boreas, doi: 10.1111/bor.12116.

Xu, D., Lu, H., Chu, G., Wu, N., Shen, C., Wang, C., Mao, L., 2014. 500-year climate cycles stacking of recent centennial warming documented in an East Asian pollen record. Sci. Rep. 4, doi: 10.1038/srep03611.

Xu, Q., Xiao, J., Li, Y., Tian, F., Nakagawa, T., 2010. Pollen-Based Quantitative Reconstruction of Holocene Climate Changes in the Daihai Lake Area, Inner Mongolia, China. J. Clim. 23, 2856-2868.

Yang, X., Wei, G., Yang, J., Jia, G, Huang, C., Xie, L., Huang, W., Argyrios, K., 2014. Paleoenvironmental shifts and precipitation variations recorded in tropical maar lake sediments during the Holocene in Southern China. Holocene 24, 1216-1225.

Yasuda, Y., Shinde, V., 2004. Monsoon and civilization. Roli, Delhi.

You, H. & Liu, J. 2012. High-resolution climate evolution derived from the sediment records of Erlongwan Maar Lake since 14 ka BP. Chin. Sci. Bull. 57, 3610-3616.

Yu, D., Liu, J., Lewis B.J., Zhou, L., Zhou, W., Fang, X., Wei, Y., Jiang, S., Dai, L., 2013. Spatial variation and temporal instability in the climate–growth relationship of Korean pine in the Changbai Mountain region of Northeast China. For. Ecol. Manage. 300, 96-105.

Yu, D., Wang, Q., Wang, Y., Zhou, W., Ding, H., Fang, X., Jiang, S, Dai, L., 2011. Climatic effects of radial growth of major tree species on Changbai Mountain. Ann. For. Sci. 68, 921-933.

Yu, G., Chen, X., Ni, J., Cheddadi, R., Guiot, J., Han, H., Harrison, S.P., Huang, C., Ke, M., Kong, Z., Li, S., Li, W., Liew, P., Liu, G., Liu, J., Liu, Q., Liu, K.-B., Prentice, I.C., Qui, W., Ren, G., Song, C., Sugita, S., Sun, X., Tang, L., van Campo, E., Xia, Y., Xu, Q., Yan, S., Yang, X., Zhao, J., Zheng, Z., 2000. Palaeovegetation of China: a pollen data-based synthesis for the mid-Holocene and Last Glacial Maximum. J. Biogeogr. 27, 635-664.

Zhang, J., Zhou, Y., Zhou, G., Xiao, C., 2014. Composition and Structure of Pinus koraiensis Mixed Forest Respond to Spatial Climatic Changes. PLoS ONE 9, e97192, doi: 10.1371/journal.pone.0097192.

Zhang, J., Chen, F., Holmes, J.A., Li, H., Guo, X., Wang, J., Li, S., Lü, Y., Zhao, Y., Qiang, M., 2011. Holocene monsoon climate documented by oxygen and carbon isotopes from lake sediments and peat bogs in China: a review and synthesis. Quat. Sci. Rev. 30, 1973-1987.

Zhang, Y., 2000. Deforestation and Forest Transition: Theory and Evidence in China, in: Palo, M., Vanhanen, H. (Eds.), Word Forests from Deforestation to Transition? Kluwer, Dordrecht, pp. 41-65.

Zhao G., Tian X., Wu, Z., 1991. Analysis and discussion on the north distributing limitation of Amur corktree, Manchurian walnut and Manchurian ash. J. Northeast For. Univ. S1, 290-295 (in Chinese with English abstract).

Zhao, Y., Yu, Z., 2012. Vegetation response to Holocene climate change in East Asian monsoon-margin region. Earth-Sci. Rev. 113, 1-10.

Zhao, Y., Yu, Z., Chen, F., 2009b. Spatial and temporal patterns of Holocene vegetation and climate changes in arid and semi-arid China. Quat. Int. 194, 6-18.

Zhao, Y., Yu, Z., Chen, F., Zhang, J., Yang, B., 2009a. Vegetation response to Holocene climate change in monsoon-influenced region of China. Earth-Sci. Rev. 97, 242-256.

Zheng, Z., Wei, J., Huang, K., Xu, Q., Lu, H., Tarasov, P., Luo, C., Beaudouin, C., Deng, Y., Pan, A., Zheng, Y., Luo, Y., Nakagawa, T., Li, C., Yang, S., Peng, H., Cheddadi, R., 2014. East Asian pollen database: modern pollen distribution and its quantitative relationship with vegetation and climate. J. Biogeogr. 41, 1819-1832.

Zhu, J., Mingram, J., Brauer, A., 2013. Early Holocene aeolian dust accumulation in northeast China recorded in varved sediments from Lake Sihailongwan. Quat. Int. 290-291, 299-312.

Zhu, T., 2003. The plants on the Changbaishan massif of China. Ke xue chu ban she, Beijing.

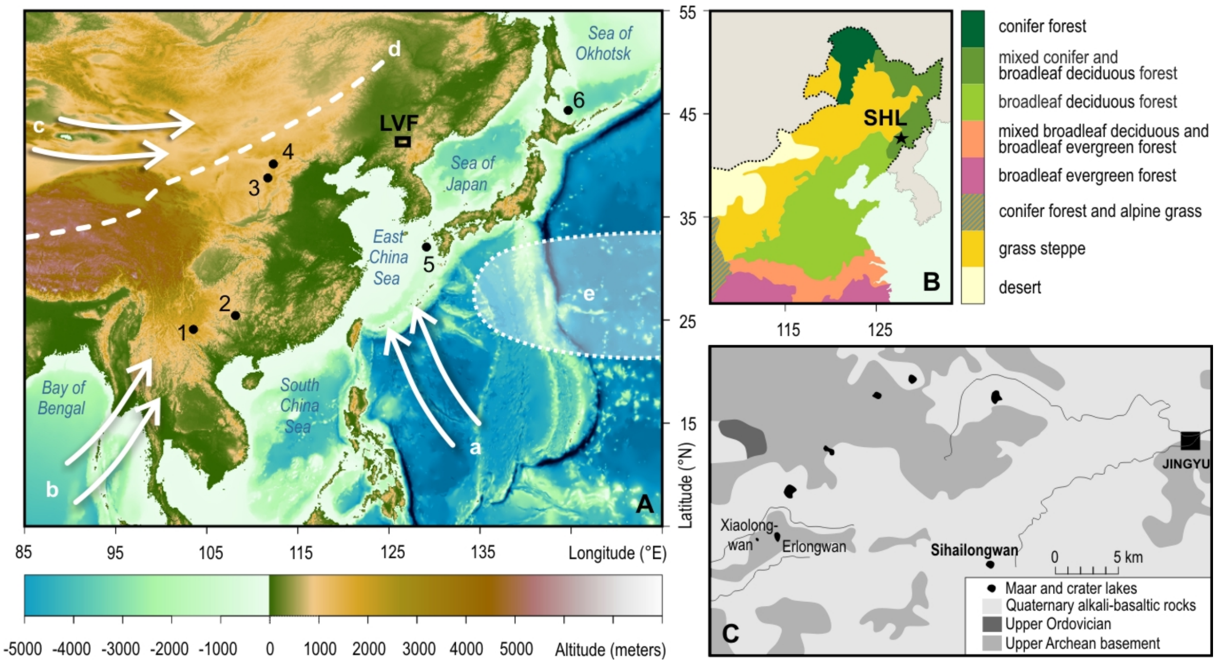

Fig. 1. (A) Map of the study area showing the study region Longgang Volcanic field (LVF), key records discussed in the text and shown in Figs. 5 and 6, respectively: (1) Xingyun Lake; (2) Dongge Cave; (3) Gonghai Lake; (4) Daihai Lake; (5) East China Sea, core Ky07-04-01, (6) Sea of Okhotsk, core Gh00-1200; and main circulation systems: (a) East Asian Summer Monsoon, (b) Indian Summer Monsoon, (c) Westerlies. The white dashed line (d) represents the limit of the modern summer monsoon (after Gao, 1962). The white-shaded area (e) marks

the Western Pacific Subtropical High. (B) Natural vegetation of north-eastern China (source: http://www.zonu.com/detail4-en/2011-07-22-14101/Natural-vegetation-of-China-1967.html). (C) Main geological units and lakes of the Longgag Volcanic Field.

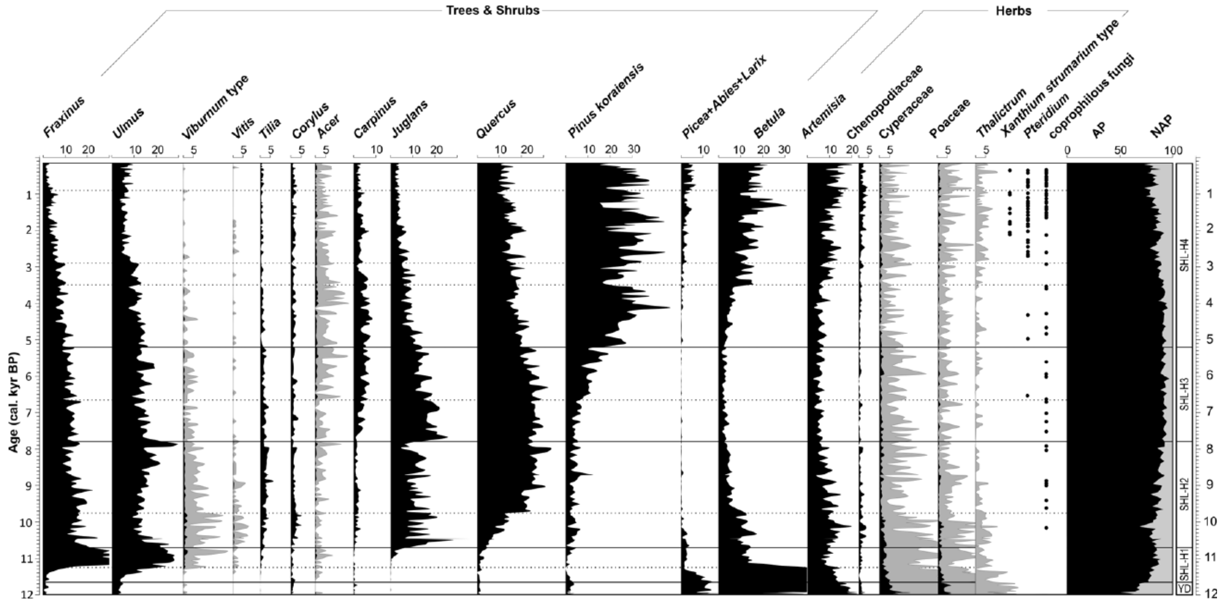

Fig. 2. Simplified pollen percentage diagram of Lake Sihailongwan (this study) plotted against the chronology presented in Schettler et al. (2006) and Stebich et al. (2009). Exaggeration (×10) is indicated by grey shading. Pollen analysts: F. Schlütz and M. Stebich.

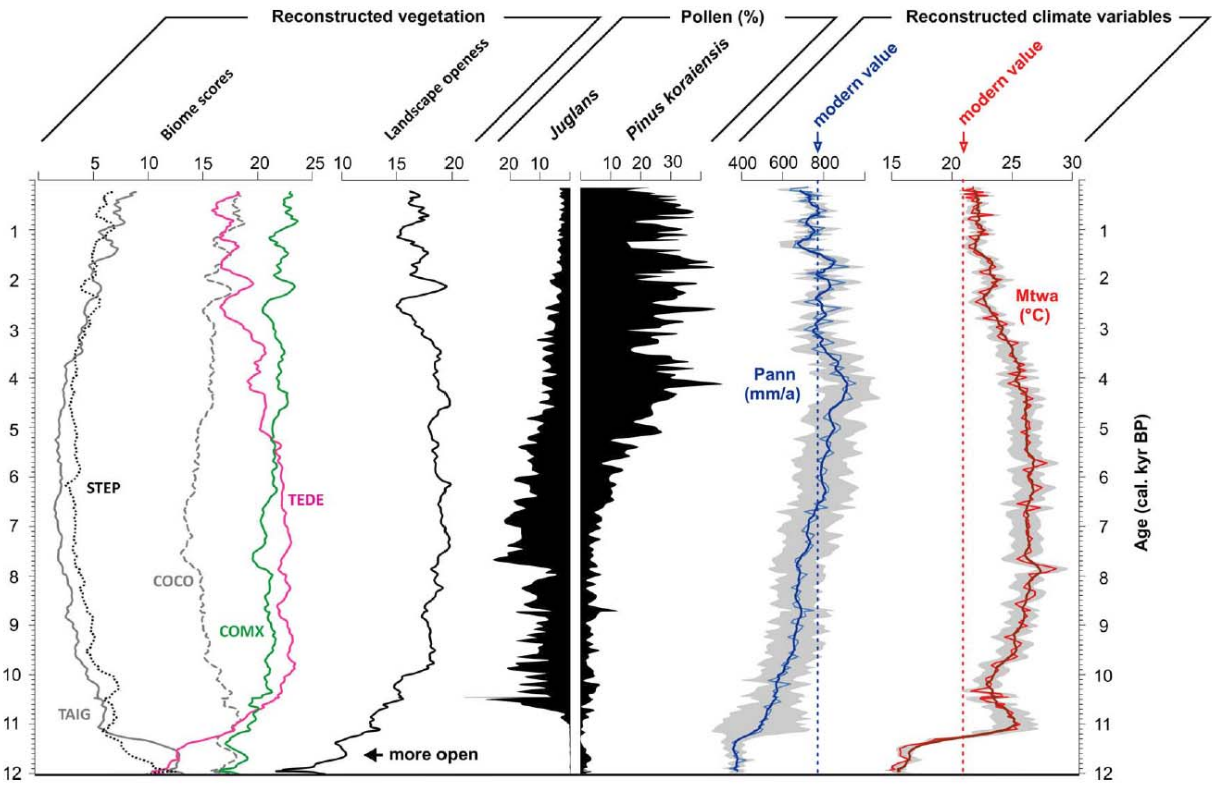

Fig. 3. Biome scores, selected pollen percentages, and climate variables of the Holocene SHL sequence. Biome scores are presented as 5-point moving averages, while their climatic interpretations are summarized in Table 1. The depicted Mtwa and Pann climate variables include 5-point moving averages (thick lines) and 2-sigma confidence intervals (grey shadow). Calculated biome scores, selected pollen taxa percentages, and pollen-derived climate variables of the Holocene SHL sequence. Biome scores are presented as 5-point moving averages, while their climatic interpretations are summarized in Table 1. The depicted Mtwa and Pann climate variables include 5-point moving averages (thick lines) and 2-sigma confidence intervals (grey shadow).

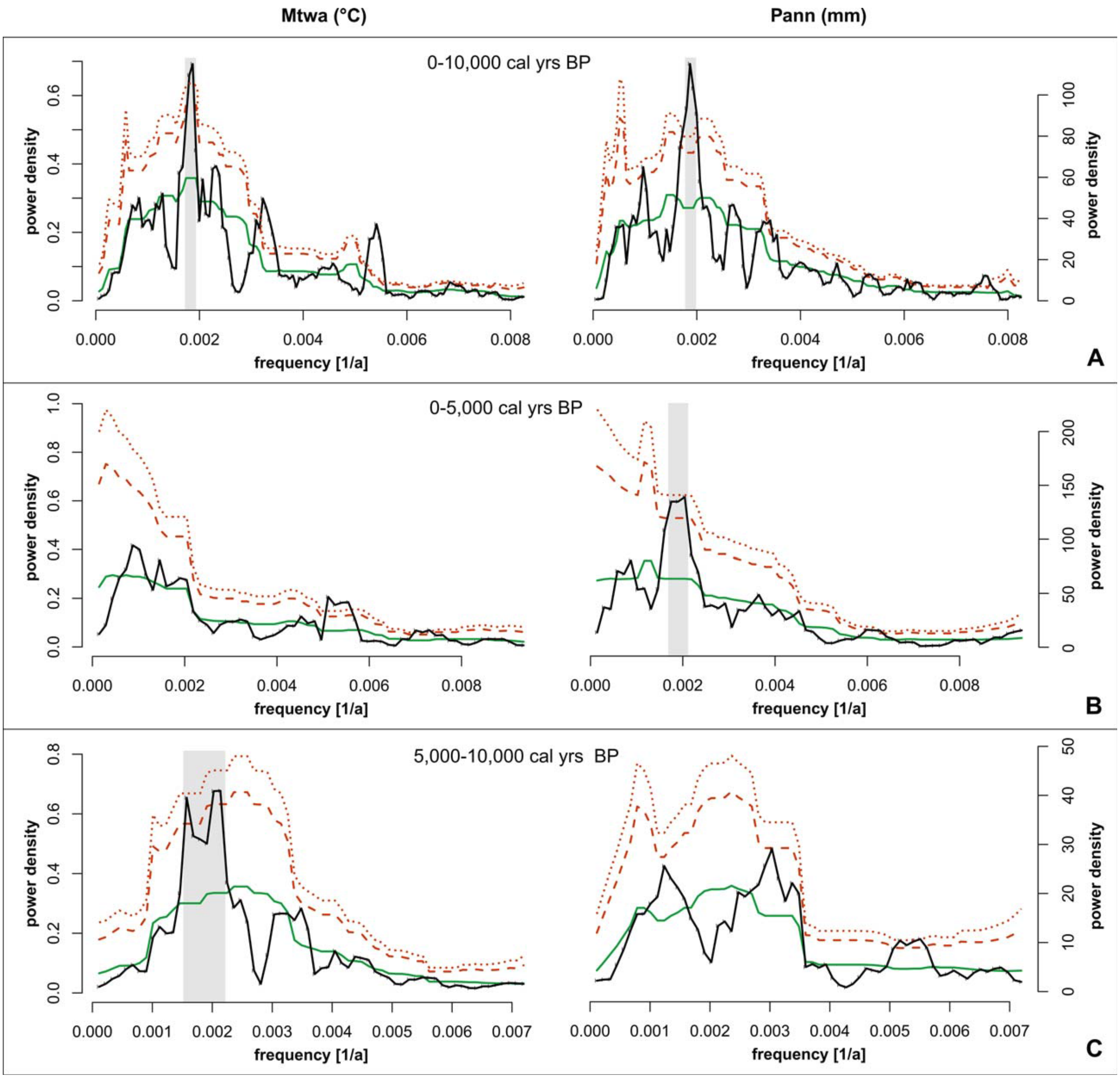

Fig. 4. Power spectra density estimates for reconstructed Mtwa and Pann (black lines) show a distinct peak around the frequency of 500^-1 years when taken over the time period from 0 to 10,000 cal. yr BP (A). The power in this band vanishes for Mtwa during the past 5,000 years (B) and for Pann between 5000 to 10,000 cal. yr BP (C). Dashed and dotted lines (red) denote the 90% (99%) confidence interval based on the background spectrum (green) which based on a χ^2 distribution with six degrees of freedom.

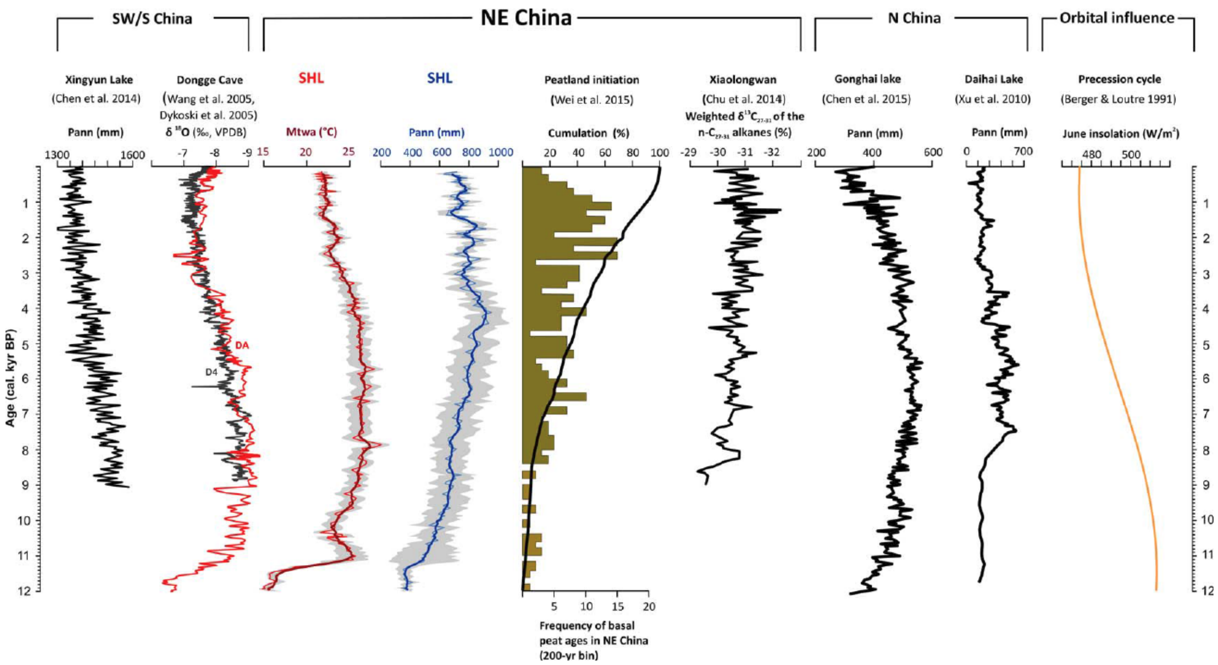

Fig. 5. The SHL pollen-derived climate variables (this study) along with the selected proxy records from SW/S and N China, and summer insolation curve. Locations of the records are given in Fig. 1.

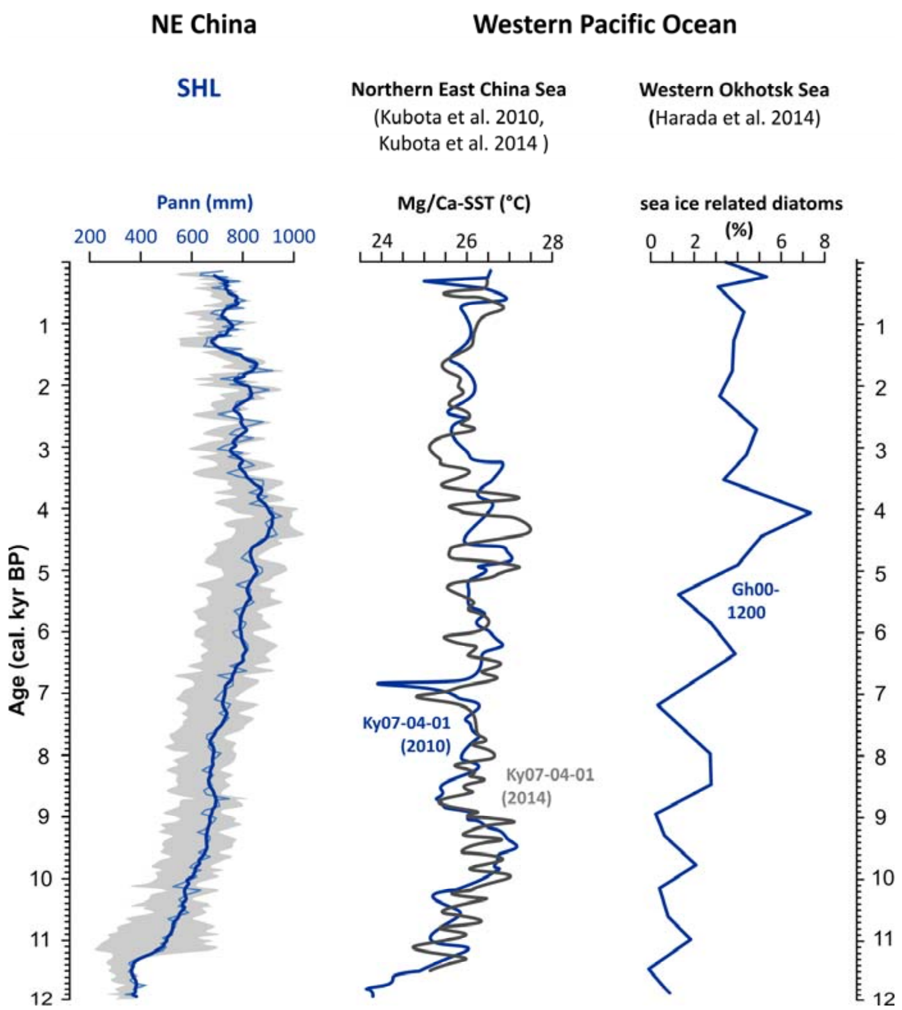

Fig. 6.

The SHL pollen-derived climate variables (this study) along with selected proxy records from the Western Pacific Ocean. Locations of the records are given in Fig. 1.

Tab. 1. Summary of climate ranges covered by the modern calibration data (Cao et al., 2014) set in comparison to the corresponding modern values at the Sihailongwan Lake.

	Modern calibration data set		Sihailongwan
	Minimum	Maximum	
Pann (mm)	35	2091	775
Tann (°C)	-12.1	25.8	2.5
Mtco (°C)	-33.8	21.7	-18.1
Mtwa (°C)	0.3	29.8	20.7

Tab. 2. Summary of the dominant plant types and of climatic requirements of the calculated SHL biome scores (abbreviations see text, GDD=growing degree days)

	Biome name and abbreviation	Dominant Plant functional types	Climatic requirements (Prentice et al. 1992, Mokhova et al. 2009)
TEDE	Temperate deciduous forests	Temperate summergreen Cool-temperate conifer Boreal summergreen	Cool winters (-2 to 0°C) and areas with colder winters (down to max. -15°C) where conditions are too dry for boreal evergreen conifers; high (>1200) GDD requirement, which indirectly excludes TEDE from regions with a very low seasonal temperature range
COMX	Cool mixed forests	Temperate summergreen Cool-temperate conifer Boreal summergreen Boreal evergreen conifer	Occurring poleward of the TEDE in climates with moderately cold winters (mean Mtco from -2°C to -15°C to -26°C); high (>1200) GDD requirement and sufficient precipitation for boreal evergreen conifers (>75%)
COCO	Cool coniferous forests	Cool-temperate conifer Boreal summergreen Boreal evergreen conifer	Mtco of -15 to -19°C separating the winter temperature tolerances of temperate summergreens and cool-temperate conifers; can also occur in climates with milder winters (-2 to -15°C), where the growing season is not warm enough for temperate deciduous trees (GDD <1200);
TAIG	Taiga	Boreal summergreen Boreal evergreen conifer	Cold winters (-19°C to -35°C) extending to somewhat warmer winters in maritime climates with GDD <900 and precipitation meeting >75% of demand
STEP	Steppe	Cool grass and shrub	Summers cooler than 22°C, precipitation meeting 28-65% of demand